JCAMECH

Vol. 48, No. 2, December 2017, pp 233-252
DOI: 10.22059/jcamech.2017.239207.172

Applications of higher order shear deformation theories on stress distribution in a five layer sandwich plate

Hamed Raissi [*], Mohammad Shishehsaz, Shapour Moradi

School of Mechanical Engineering, Shahid Chamran University of Ahvaz, Ahvaz, Iran.

Received: 5 Aug. 2017, Accepted: 1 Sep. 2017

Abstract

In this paper, layerwise theory (LT) along with the first, second and third-order shear deformation theories (FSDT, SSDT and TSDT) are used to determine the stress distribution in a simply supported square sandwich plate subjected to a uniformly distributed load. Two functionally graded (FG) face sheets encapsulate an elastomeric core while two epoxy adhesive layers adhere the core to the face sheets. The sandwich plate is assumed to be symmetric with respect to its core mid-plane. First, second and third-order shear deformation theories are used to model shear distribution in the adhesive layers as well as others. Results obtained from the three theories are compared with those of finite element solution. Results indicate that finite element analysis (FEA) and LT based on the first, second and third-order shear deformation theories give almost the same estimations on planar stresses. Moreover, the out-of-plane shear stresses obtained by FEA, are slightly different from those of LT based on FSDT. The differences are decreased on using LT based on SSDT or TSDT. Additionally, SSDT and TSDT predict almost the same distribution for the two planer stress and out-of-plane shear stress components along the face sheet thickness. Furthermore, third-order shear deformation theory seems to be more appropriate for prediction of out-of-plane shear stress at lower values of a/*h* ratio.

Keywords: Stress distribution, Layerwise theory, Second-order shear deformation, Third-order shear deformation, Sandwich plate.

[*] Corresponding author.
E-mail address: h-raissi@phdstu.scu.ac.ir

1. Introduction

Most of the literature available on the sandwich composite plates which is based on LT have dealt with FSDT. Liu et al. [1] used differential quadrature finite element method (DQFEM) along with LT based on an expansion of Mindlin's first-order shear deformation theory to study laminated composites and sandwich plates. The DQFEM solutions were compared with various models in the literature. Very good agreements with exact solutions that were based on a similar LT were observed. Fares et al. [2] studied stress distribution in a plate based on LT while its thickness was divided into n layers. They assumed a continuous change in displacement along the thickness. Application of FSDT theory was also used by Thai et al. [3], Ferreira et al. [4] and Roque et al. [5] to perform the static deformation and vibrational analysis of a sandwich plates by means of LT. Application of functional graded materials were used by Farahmand and Atai [6], Afshin et al [7] and Goodarzi et.al [8] to analyze spherical vessel, rotating thick cylindrical pressure vessels and nanoplates, respectively. Gharibi et al. [9] studied elastic analysis of FG rotating thick cylindrical pressure vessels by using power series method of frobenius. The vessel is considered in both plane stress and plane strain conditions. They illustrate that the inhomogeneity constant provides a major effects on the mechanical behaviors of the vessel. In another work, Mantari et al. [10] performed the static and dynamic analysis of laminated composite and sandwich plates and shells, using a new higher-order shear deformation theory. The governing equations and boundary conditions were derived using principle of virtual work. The static and dynamic results were then presented for cylindrical and spherical shells and plates based on simply supported boundary conditions. The accuracy of their results were verified using the available results in the literature. In Ref. [11], Nguyen-Xuan et al. performed isogeometric finite element analysis of a composite sandwich plate, using a higher-order shear deformation theory. The static, dynamic and buckling behavior of rectangular and circular plates were investigated based on different boundary conditions. They observed good agreements between their results and work of others which were based on analytical solutions.

Many researches have carried out variety of works related to nanostructures elements such as nanorod, nanobeam and nanoplates. Goodarzi et al. [12] studied thermo-mechanical vibration analysis of FG circular and annular nanoplate based on the visco-pasternak foundation by using strain gradient theory. Farajpour et al. [13] studied vibration of piezoelectric nanofilm based electromechanical sensors via higher order nonlocal strain gradient theory. In this research by using higher order nan-local elasticity, strain gradient theory and Hamilton's principle, the equations of motion are derived. Farajpour et al. [14-16] studied surface effects, large amplitude vibration and buckling analysis of nanoplates subjected to external electric and magnetic potentials. Mohammadi et al. [17] studied shear buckling of orthotropic rectangular plate. In this work, nan-local elasticity theory studied to determined shear buckling of orthotropic single layered graphene sheets. Mohammadi et al. [18, 19] studied the effect of shear in plane load on the vibration of circular, annular and rectangular plates. In these research by using nonlocal elasticity theory vibration analysis of orthotropic single layered graphene sheets studied. In Ref [20], Farajpour et al. studied buckling analysis of orthotropic nanoplates in thermal environment. In this investigation the higher order nonlocal strain gradient theory used to determine the influences of higher order deformation. Ghabezi and Farahani [21] studied adhesive bonded joint reinforcement by incorporation of nano alumina particles. This paper was experimental investigation on the effects of the addition nanoparticles to woven. The shear tensile test shows that variation of the nanoparticles led to increase the joint strength.

Finite element analysis of laminated composite plates using a higher-order shear deformation theory with assumed strains was performed by Lee and Kim [22]. They used a new four-node laminated plate by using a higher-order shear deformation theory. Several numerical examples were carried out and their results were compared with work of others. They concluded that their proposed method was very effective to remove the locking phenomenon and produces reliable numerical solutions for most laminated composite plate structures. In Ref. [23], Houari et al. developed a new higher-order shear and normal deformation theory to simulate the thermo elastic bending of functionally graded (FG) material sandwich plates. Their theory accounted for both shear deformation and thickness stretching effects using a sinusoidal variation in all displacements across the thickness without requiring any shear correction factor. Numerical examples were presented to verify the accuracy of the proposed theory. Dynamic behavior of fiber reinforced plastic sandwich plates with PVC foam core was investigated by Meunier and Shenoi [24]. The deduced equations of motion which included the viscoelastic properties of the constitutive materials were used to determine the natural frequencies and modal loss factors of a specific composite sandwich plate. They concluded that to determine the dynamic response of fiber reinforced sandwich structures, the viscoelastic properties of constitutive materials and their temperature and frequency dependency should not be omitted. Shishesaz et al. [25] studied local buckling of composite plates subjected to compressional load. In this research, the proposed analysis will predict the delamination shape

of a composite plate during delamination process in post-buckling mode.

Thai et al. [26], presented a generalized layerwise higher-order shear deformation theory for laminated composite and sandwich plates. Their work introduced a higher-order shear deformation theory in each layer such that the continuity in displacement and transverse shear stresses at the layer interfaces was ensured. Similar to the first and higher-order shear deformation theories, their method required only five variables. In comparison with the shear deformation theories based on the equivalent single layer, they claimed that their proposed theory was capable of producing a higher accuracy for inter-laminar shear stresses. Sarangan and Singh [27] studied higher-order closed-form solution of laminated composite and sandwich plates. In their work, new shear deformation theories were developed to analyze the static, buckling and free vibration responses of laminated composites and sandwich plates using Navier closed form solution technique. The governing differential equations and boundary conditions were obtained using the virtual work principle. Their results showed that the proposed shear strain functions have significant effects on structural responses.

In spite of the extensive literature available on behavior of sandwich composite plates, there still remains other questions which yet have to be answered. For this purpose, this work deals with stress distribution in a five-layer rectangular sandwich composite plate composed of a central polymeric core adhered to FG cover sheets by means of two adhesive layers. The whole structure is subjected to a uniformly distributed transverse load and is simply supported on all four edges. Since any excessive stress in the adhesive layers may lead to a bond separation between the face sheets and the core, and hence failure of the overall structure, it becomes very important to have a full understanding on distribution of stresses in each layer and the important factors influencing their magnitude, and possibly their locations. This leads to a better understanding on the behavior of the overall structure and hence, can prevent any possible failure due to the application of any excessive load.

Although FSDT predicted accurate results on planer stresses, magnitudes of out-of-plane shear stresses which appeared to be constant along the adhesive thickness based on FSDT, did not quite match those of finite element results and work of others. In this text, LT along with higher-order shear deformation theories (second and third orders) will be used to investigate their applicability and effect on stress distribution in a five-layer sandwich composite plate. The effect of other factors on final results will be also investigated. The major advantage of LT along with higher-order shear deformation theories compared to FSDT is that to predict accurate results on out-of-plane shear stresses. But the major limitation of the theory appeared when the thickness of the sandwich plate becoming large or the ratio of the sandwich plate thickness to its length becoming large.

2. Derivation of the governing equations

In this section, the governing equations relating stresses to strains in a five-layer, square, simply supported sandwich plate based on LT and SSDT or TSDT are derived. Figure 1 illustrates the sandwich plate with two FG face sheets under uniformly distributed transverse load q_0. The modulus of elasticity of each face sheets along its thickness is defined by Eq. (1). It is assumed that the Poisson's ratio of each face sheet is constant. In Eq. (1), indices *c* and *m* correspond to the ceramic and metal, *n* is the material number, and *E* is the elastic modulus. V_c corresponds to the volume fraction of ceramic composition in metal. Moreover, h_1, h_2 and h_3 correspond to the thickness of the face sheets, adhesive layers and core, respectively (see Fig. 1).

Based on SSDT and TSDT, planar displacement components along the thickness of each layer change according to the second and third-order polynomials, respectively. These polynomials are written in terms *z* coordinate described locally in each layer along the thickness of the plate. Assuming a continuous displacement across the layers, the displacement fields in each layer based on the SSDT and TSDT are deduced and given in appendices *A* and *B*, respectively.

$$E(z)=\left(E_c-E_m\right)V_c+E_m, \qquad \text{where} \quad V_c=\begin{cases}\left(\dfrac{z-\left(\frac{h_1}{2}+h_2+\frac{h_3}{2}\right)}{h_1}+\dfrac{1}{2}\right)^n & \text{Top face sheet}\\ \left(\dfrac{z+\left(\frac{h_1}{2}+h_2+\frac{h_3}{2}\right)}{h_1}-\dfrac{1}{2}\right)^n & \text{Bottom face sheet}\end{cases} \tag{1}$$

Here, $u^{(k)}$, $v^{(k)}$ and $w^{(k)}$ indicate the displacement components along *x*, *y* and *z* directions in the k^{th} layer, respectively. Numbering of the layers is shown in Fig. 1. Moreover, *u* and *v* are the corresponding displacement components measured along *x* and *y* directions at the core mid-plane (*z*=0), respectively. Additionally, it is assumed that the out-of-plane displacement $w^{(k)}$ is only a function of *x* and *y* and a perfect bond exists between all layers. The adhesive layers are assumed to be void free. Based on linear elasticity, the strain components in the k^{th} layer can be written in terms of displacements, as in Eqs. (2). Substituting for displacement components from Appendices *A* and *B* in Eqs. (2), the strain vector in each layer of the five-layer composite sandwich plate, for the two postulated models (SSDT and TSDT), may be

written as in Eqs. (3). In these equations, to apply SSDT, $a_1=1$, $a_2=0$ while for TSDT, $a_1=0$ and $a_2=1$. Moreover, the components $\varepsilon_x^{m(k)}$, $\varepsilon_y^{m(k)}$, $\gamma_{xy}^{m(k)}$, $\gamma_{xz}^{m(k)}$ and $\gamma_{yz}^{m(k)}$ represent the m^{th}-order polynomial coefficients of the strains for the k^{th} layer. The stress-strain relationship in the k^{th} layer may be written in terms of Eq. (4). Here, $\left[Q_{ij}^{(k)}\right]$ is the stiffness matrix of the k^{th} layer. In Eq. (5), $E^{(k)}$, $G^{(k)}$ and $\upsilon^{(k)}$ correspond to the modulus of elasticity, shear modulus and Poisson's ratio of the k^{th} layer respectively.

$$\varepsilon_x^{(k)}=\frac{\partial u^{(k)}}{\partial x};\ \varepsilon_y^{(k)}=\frac{\partial v^{(k)}}{\partial y}\ ;\ \varepsilon_z^{(k)}=0;\ \gamma_{yz}^{(k)}=\frac{\partial v^{(k)}}{\partial z}+\frac{\partial w}{\partial y};\ \gamma_{xz}^{(k)}=\frac{\partial u^{(k)}}{\partial z}+\frac{\partial w}{\partial x}\ ;\ \gamma_{xy}^{(k)}=\frac{\partial u^{(k)}}{\partial y}+\frac{\partial v^{(k)}}{\partial x} \tag{2}$$

$$\begin{bmatrix}\varepsilon_x^{(k)}\\ \varepsilon_y^{(k)}\\ \gamma_{xy}^{(k)}\end{bmatrix}=\begin{bmatrix}\varepsilon_x^{0(k)}\\ \varepsilon_y^{0(k)}\\ \gamma_{xy}^{0(k)}\end{bmatrix}+z^{(k)}\begin{bmatrix}\varepsilon_x^{1(k)}\\ \varepsilon_y^{1(k)}\\ \gamma_{xy}^{1(k)}\end{bmatrix}+a_1z^{(k)2}\begin{bmatrix}\varepsilon_x^{2(k)}\\ \varepsilon_y^{2(k)}\\ \gamma_{xy}^{2(k)}\end{bmatrix}+a_2z^{(k)3}\begin{bmatrix}\varepsilon_x^{3(k)}\\ \varepsilon_y^{3(k)}\\ \gamma_{xy}^{3(k)}\end{bmatrix};\ \begin{bmatrix}\gamma_{yz}^{(k)}\\ \gamma_{xz}^{(k)}\end{bmatrix}=\begin{bmatrix}\gamma_{yz}^{0(k)}\\ \gamma_{xz}^{0(k)}\end{bmatrix}+a_1z^{(k)}\begin{bmatrix}\gamma_{yz}^{1(k)}\\ \gamma_{xz}^{1(k)}\end{bmatrix}+a_2z^{(k)2}\begin{bmatrix}\gamma_{yz}^{2(k)}\\ \gamma_{xz}^{2(k)}\end{bmatrix} \tag{3}$$

$$\begin{bmatrix}\sigma_x^{(k)}\\ \sigma_y^{(k)}\\ \tau_{yz}^{(k)}\\ \tau_{xz}^{(k)}\\ \tau_{xy}^{(k)}\end{bmatrix}=\left[Q_{ij}^{(k)}\right]\begin{bmatrix}\varepsilon_x^{(k)}\\ \varepsilon_y^{(k)}\\ \gamma_{yz}^{(k)}\\ \gamma_{xz}^{(k)}\\ \gamma_{xy}^{(k)}\end{bmatrix}\qquad\text{where}\qquad\left[Q_{ij}^{(k)}\right]=\begin{bmatrix}Q_{11}^{(k)} & Q_{12}^{(k)} & 0 & 0 & 0\\ Q_{12}^{(k)} & Q_{22}^{(k)} & 0 & 0 & 0\\ 0 & 0 & Q_{44}^{(k)} & 0 & 0\\ 0 & 0 & 0 & Q_{55}^{(k)} & 0\\ 0 & 0 & 0 & 0 & Q_{66}^{(k)}\end{bmatrix} \tag{4}$$

$$Q_{11}^{(k)}=Q_{22}^{(k)}=\frac{E^{(k)}}{1-\upsilon^{(k)2}};\ Q_{12}^{(k)}=\upsilon^{(k)}Q_{11}^{(k)};\ Q_{44}^{(k)}=Q_{55}^{(k)}=Q_{66}^{(k)}=G^{(k)} \tag{5}$$

$$\delta\pi=\int_\Omega\left\{\sum_{k=1}^{5}\int_{-\frac{h_k}{2}}^{\frac{h_k}{2}}\left[\begin{array}{l}\sigma_x\left[\delta\varepsilon_x^{0(k)}+z^{(k)}\delta\varepsilon_x^{1(k)}+a_1z^{(k)2}\delta\varepsilon_x^{2(k)}+a_2z^{(k)3}\delta\varepsilon_x^{3(k)}\right]+\\ \sigma_y\left[\delta\varepsilon_y^{0(k)}+z^{(k)}\delta\varepsilon_y^{1(k)}+a_1z^{(k)2}\delta\varepsilon_y^{2(k)}+a_2z^{(k)3}\delta\varepsilon_y^{3(k)}\right]+\\ \tau_{xy}\left[\delta\gamma_{xy}^{0(k)}+z^{(k)}\delta\gamma_{xy}^{1(k)}+a_1z^{(k)2}\delta\gamma_{xy}^{2(k)}+a_2z^{(k)3}\delta\gamma_{xy}^{3(k)}\right]+\\ \tau_{yz}\left[\delta\gamma_{yz}^{0(k)}+a_1z^{(k)}\delta\gamma_{yz}^{1(k)}+a_2z^{(k)2}\delta\gamma_{yz}^{2(k)}\right]+\\ \tau_{xz}\left[\delta\gamma_{xz}^{0(k)}+a_1z^{(k)}\delta\gamma_{xz}^{1(k)}+a_2z^{(k)2}\delta\gamma_{xz}^{2(k)}\right]-q_o\delta w\end{array}\right]dz\right\}dxdy=0 \tag{6}$$

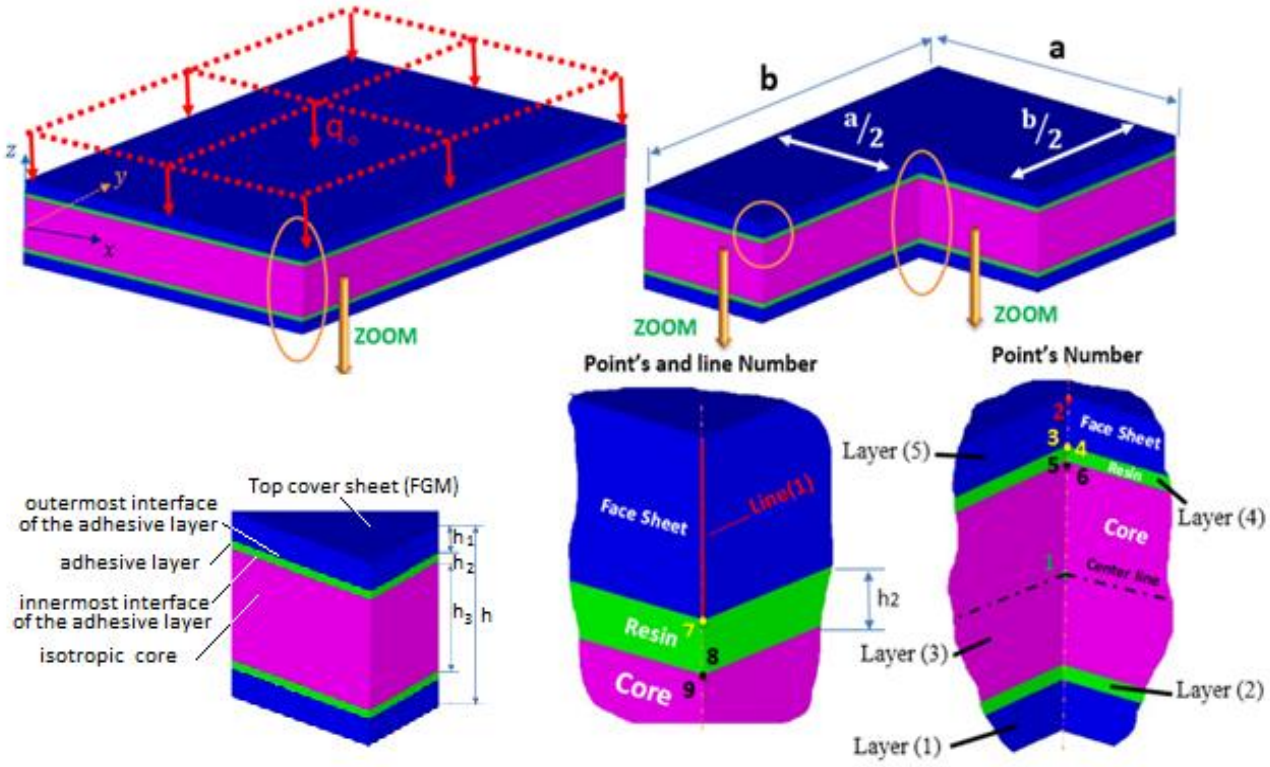

Fig. 1. The five-layer simply supported sandwich plate with functionally graded face sheets under uniformly distributed load q_o.

Writing the expression for potential energy and setting its variation equal to zero, as in Eq. (6), the equilibrium equations based on SSDT and TSDT are extracted and presented in Appendices *C* and *D*, respectively. In Eq. (6), q_0 is the magnitude of the uniform load applied to the top surface of the sandwich plate. Additionally, parameters $N_i^{(k)}$, $M_i^{(k)}$, $L_i^{(k)}$ and $P_i^{(k)}$ (i=1, 2, 6), $Q_j^{(k)}$, $K_j^{(k)}$ and $R_j^{(k)}$ (j=1, 2) given in Appendices *C* and *D* are fully expressed in Appendix *E*. Since simply support boundary condition is used on all four edges, then the displacement components and curvatures can be defined as in Eqs. (7). In these equations, u_{mn}, v_{mn}, w_{mn}, $\phi_{x\,mn}^{(k)}$, $\phi_{y\,mn}^{(k)}$, $\psi_{x\,mn}^{(k)}$ and $\psi_{y\,mn}^{(k)}$ are the constants yet to be determined.

$$u=\sum_{m=1}^{\infty}\sum_{n=1}^{\infty}u_{mn}\cos(\alpha x)\sin(\beta y);\ v=\sum_{m=1}^{\infty}\sum_{n=1}^{\infty}v_{mn}\sin(\alpha x)\cos(\beta y);\ w=\sum_{m=1}^{\infty}\sum_{n=1}^{\infty}w_{mn}\sin(\alpha x)\sin(\beta y) \tag{7a}$$

$$\phi_x^{(k)}=\sum_{m=1}^{\infty}\sum_{n=1}^{\infty}\phi_{x\,mn}^{(k)}\cos(\alpha x)\sin(\beta y);\ \phi_y^{(k)}=\sum_{m=1}^{\infty}\sum_{n=1}^{\infty}\phi_{y\,mn}^{(k)}\sin(\alpha x)\cos(\beta y) \tag{7b}$$

$$\psi_x^{(k)}=\sum_{m=1}^{\infty}\sum_{n=1}^{\infty}\psi_{x\,mn}^{(k)}\cos(\alpha x)\sin(\beta y);\ \psi_y^{(k)}=\sum_{m=1}^{\infty}\sum_{n=1}^{\infty}\psi_{y\,mn}^{(k)}\sin(\alpha x)\cos(\beta y) \tag{7c}$$

Where

$$0\le x\le a,\ 0\le y\le b,\ \alpha=\frac{m\pi}{a},\ \beta=\frac{n\pi}{b} \tag{7d}$$

On using Eqs. (7) in conjunction with displacements and rotational components given in Appendices *A* and *B*, and then substituting the results back in Eqs. (2), strains in each layer are determined. Applying Fourier series to define this uniform load, one may write;

$$q(x,y)=\sum_{m=1}^{\infty}\sum_{n=1}^{\infty}B_{mn}\sin(\alpha x)\sin(\beta y) \quad \text{where} \quad B_{mn}=\begin{cases}\dfrac{16q_o}{mn\pi^2} & m \text{ and } n \text{ are odd.}\\ 0 & m \text{ or } n \text{ are even.}\end{cases} \tag{8}$$

Based on the second and third-order shear deformation theories along with LT, a family of forces and moments are developed which are given in Appendix *E*. Here, matrices *A*, *B*, *D*, *E*, *F*, *H*, *J* and *L* which are introduced in equilibrium equations of each layer are expressed in Eqs. (E3) and (E4). Coefficients $(\ )_{mn}$ in Eqs. (7) are obtained by solving the system of equations given in Appendices *C* and *D*.

3. Numerical results and discussion

Based on the governing equations derived in the previous section, stress distribution in a five-layer sandwich plate is now investigated. Proper relations are used to deduce the results which are based on each one of the two shear deformation theories (SSDT or TSDT). The results based on FSDT and finite element findings are imported from the first part of the paper for further comparison.

3.1. Three-layer sandwich plate

To find the effect of second and third-order shear deformation theories on final results, as the first step, a three-layer sandwich plate (with no adhesive layer) is postulated as shown in Fig. 2. Here, the simply supported, square, orthotropic sandwich plate is subjected to a uniformly distributed transverse load q_0 on its top face. The geometric dimensions of the sandwich plate are selected such that its total thickness is ten percent of its overall length. Moreover, the thickness of each face sheet is assumed to be equal to 10 percent of the overall thickness. Allowing the thickness of each adhesive layer to approach zero and neglecting the terms associated with these two layers in current formulations, a solution to displacement field "*w*" and stress components σ_x, σ_y and τ_{xz} are obtained based on LT along with FSDT, SSDT, and TSDT. The stiffness matrices for the core and face sheets were selected according to Eqs. (9) [28], where R is assumed to be a constant number.

The finite element findings and the non-dimensional results for different points based on three dimensional elasticity deduced from Ref. [28] are superimposed for further comparison. The results at five different points (1-5) are shown in Table 1. These values are non-dimensionalized according to Eq. (10). The geometric positions of these points are given in Table 2. The results in Table 1 are deduces for three different values of *R*. It is observed that the order of accuracy in prediction of planar stress components $\bar{\sigma}_x$ and $\bar{\sigma}_y$ (compared to 3-D elasticity solution) at each one of these points, based on FSDT, SSDT, and TSDT is almost the same for all values of R listed in this table.

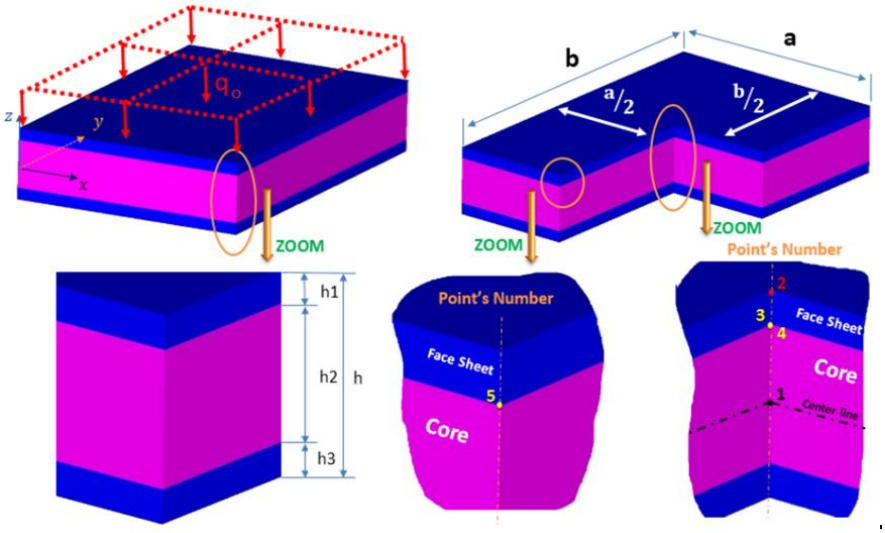

Fig. 2. Three-layer simply supported sandwich plate.

Table 1. Comparison of the results based on LT along with FSDT, SSDT and TSDT and those of analytical solution obtained from Ref. [28] for h_1/h=0.1,h_2/h=0.8,h_3/h=0.1 (three layer composite sandwich plate).

$R=\frac{[Q]_{face\,sheet}}{[Q]_{Core}}$		$\bar{w}$	$\bar{\sigma}_x$			$\bar{\sigma}_y$			$\bar{\tau}_{xz}$
		Point 1	Point 2	Point 3	Point 4	Point 2	Point 3	Point 4	Point 5
1	Ref. [28]	688.58	36.021	28.538	28.538	22.210	17.669	17.669	-1.9826
	LT FSDT	705.08	37.471	29.924	29.924	21.827	17.460	17.460	-1.7839
	% Difference	2.40	4.03	4.86	4.86	-1.72	-1.18	-1.18	-10.02
	LT SSDT	705.26	37.467	29.922	29.922	21.828	17.461	17.461	-1.9650
	% Difference	2.42	4.01	4.85	4.85	-1.72	-1.18	-1.18	-0.89
	LT TSDT	707.52	37.506	29.942	29.942	21.860	17.483	17.483	-1.8917
	% Difference	2.75	4.12	4.92	4.92	-1.58	-1.05	-1.05	-4.58
5	Ref. [28]	258.97	60.353	46.623	9.3402	38.491	30.097	6.1607	-3.2675
	LT FSDT	263.04	62.155	49.435	9.8871	37.974	30.368	6.0737	-3.1839
	% Difference	1.57	2.99	6.03	5.86	-1.34	0.90	-1.41	-2.56
	LT SSDT	263.14	62.146	49.431	9.8861	37.978	30.371	6.0742	-3.1767
	% Difference	1.61	2.97	6.02	5.84	-1.33	0.91	-1.40	-2.78
	LT TSDT	263.31	62.193	49.476	9.8951	38.003	30.389	6.0778	-3.3521
	% Difference	1.68	3.05	6.12	5.94	-1.27	0.97	-1.35	2.59
10	Ref. [28]	159.38	63.322	48.857	4.903	43.566	33.413	3.4995	-3.5154
	LT FSDT	160.31	66.398	52.484	5.2484	42.892	34.274	3.4274	-3.6555
	% Difference	0.58	4.86	7.42	7.04	-1.55	2.58	-2.06	3.99
	LT SSDT	160.37	66.389	52.479	5.2479	42.896	34.277	3.4277	-3.6541
	% Difference	0.62	4.84	7.41	7.03	-1.54	2.59	-2.05	3.94
	LT TSDT	160.39	66.423	52.536	5.2536	42.916	34.292	3.4291	-3.9118
	% Difference	0.63	4.90	7.53	7.15	-1.49	2.63	-2.01	11.28

$$Q_{facesheet} = RQ_{core} \qquad \text{where} \qquad Q_{core} = \begin{bmatrix} 3.802 & 0.879 & 0 & 0 & 0 \\ 0.879 & 1.996 & 0 & 0 & 0 \\ 0 & 0 & 1.015 & 0 & 0 \\ 0 & 0 & 0 & 0.608 & 0 \\ 0 & 0 & 0 & 0 & 1 \end{bmatrix} \tag{9}$$

$$\bar{w} = -\frac{w\left(\frac{a}{2},\frac{b}{2},0\right)Q_{core}(1,1)}{hq_o}, \quad \bar{\sigma}_x = \frac{\sigma_x}{q_o}, \quad \bar{\sigma}_y = \frac{\sigma_y}{q_o}, \quad \bar{\tau}_{xz} = \frac{\tau_{xz}}{q_o} \tag{10}$$

Table 2. Geometric position and location of points 1-5 defined in Table 1, according to the coordinate system shown in Fig. 2.

Point's number	1	2	3	4	5
Location, on the	Core	Face sheet	Face sheet	Core	Face sheet
x Coordinate	a/2	a/2	a/2	a/2	a/2
y Coordinate	b/2	b/2	b/2	b/2	0
z Coordinate	0	$h/2$	$h_2/2$	$h_2/2$	$h_2/2$

Compared to 3-D elasticity solution, the out-of-plane shear stress component $\bar{\tau}_{xz}$ at point 5 is well predicted by SSDT compared to the other two. Consequently, it appears that LT along with SSDT is well capable of predicting the out-of-plane shear stress component $\bar{\tau}_{xz}$ as well as other stress components $\bar{\sigma}_x$ and $\bar{\sigma}_y$ and deflection $\bar{w}$, in a three layer sandwich composite plate.

3.2. Five-layer sandwich plate

To further examine the applicability of LT along with higher-order shear deformation theories to a five-layer sandwich composite plate, two adhesive layers between the core and face sheets were added to the previous model. The postulated model which is shown in Fig. 1, is simply supported on all four edges and subjected to a uniformly distributed transverse load q_0 on its top face. The resulting square sandwich plate is assumed to be symmetric with respect to its core mid-plane. The mechanical properties of each layer are defined in Table 3. Tables 4 to 6 compare the results on deflection $\bar{w}$, $\bar{\sigma}_x$ and $\bar{\tau}_{xz}$, based on LT along with SSDT and TSDT and those of FEA and FSDT. Here, due to symmetry in geometry of the plate and loading, $\bar{\sigma}_x = \bar{\sigma}_y$. For the assumed values of h_1, h_2 and h_3 in Table 4, based on n=1, it is observed that the resulting values for $\bar{w}$, $\bar{\sigma}_x$ and $\bar{\tau}_{xz}$, which are obtained based on the second-order and third-order shear deformation theories, match those of FEA and FSDT. The percentage differences between FE results and those of shear deformation theories seem to be reduced for higher values of a/*h*, almost at all points given in Table 4. The accuracy in values of $\bar{\tau}_{xz}$ along line 1 (in the top face sheet as in Fig. 1) increases with implementation of higher-order shear deformation theories in current analysis. At points 7, 8 and 9 (these points lie in the top adhesive layer), application of higher-order shear deformation theories does not seem to improve much the values of $\bar{\tau}_{xz}$ at the core-adhesive and adhesive-cover sheet interfaces. However, higher values of a/*h* result in higher values of $\bar{w}$, $\bar{\sigma}_x$ and $\bar{\tau}_{xz}$, and their accuracy.

Table 3. Mechanical properties of the five-layer sandwich plate.

Sheet type	Mechanical properties
Face sheet $(AL - AL_2O_3)$ [29]	E_m=70GPa; E_c=380GPa; ν_m=ν_c=0.3
Epoxy (Epo-tek 301-2) [30]	E=3.664GPa; ν=0.3
Core (Elastomeric Foam code 4) [31, 32]	E=1.5GPa; ν=0.463

Figure 3 shows the non-dimensional changes in planer stress ($\bar{\sigma}_x$) in the top face sheet along its thickness direction based on the three shear deformation theories and FEA. Two different values of n = 0.5 and n = 2.0 are selected for this purpose (see Figs. 3(a) and (b)). The upper and bottom layers of the top cover sheet experience

the same absolute values of in-plane stress $\bar{\sigma}_x$, as the composite plate undergoes bending due to the applied transverse load q_0. For the selected values of n, LT along with FSDT seems to predict similar values for $\bar{\sigma}_x$ as the other shear stress theories and FEA do. Similar results are obtained for other cover sheet thicknesses (see Figs. 3(c) and (d)). According to Fig. 3(d), a thicker cover sheet results in lower values of $\bar{\sigma}_x$. Variations in $\bar{\sigma}_x$ and $\bar{\tau}_{xz}$ in the top face sheet along *x* and *z* directions at *y*=b/2, are shown in Fig. 4. Clearly, one can observe that SSDT and TSDT almost predict similar distributions for these two stress components along the foregoing directions.

The effect of cover sheet thickness on deflection $\bar{w}$, $\bar{\sigma}_x$ and $\bar{\tau}_{xz}$ at different points is shown in Table 5. According to these results, a sandwich composite plate with a thicker cover sheet experiences lower values of $\bar{w}$ and $\bar{\sigma}_x$ (at the mid-center of the plate), while $\bar{\tau}_{xz}$ seems to be slightly increased at points which are located on each of its interfaces (see the results for points 7-9 and those on line 1).

The effect of cover sheet thickness on deflection $\bar{w}$, $\bar{\sigma}_x$ and $\bar{\tau}_{xz}$ at different points is shown in Table 5. According to these results, a sandwich composite plate with a thicker cover sheet experiences lower values of $\bar{w}$ and $\bar{\sigma}_x$ (at the mid-center of the plate), while $\bar{\tau}_{xz}$ seems to be slightly increased at points which are located on each of its interfaces (see the results for points 7-9 and those on line 1). Figure 5 shows the non-dimensional changes in out-of-plane shear stress $\bar{\tau}_{xz}$ in the top face sheet along its thickness. Here, it has been assumed that *n*=1. For a/*h*=15, the second and third-order shear deformation theories seem to predict almost the same distributions for $\bar{\tau}_{xz}$. These results appear to be slightly different from those of FEA. According to this figure, higher values of a/*h* (20 and 30), result in higher values of $\bar{\tau}_{xz}$ in the top face sheet. The corresponding results predicted by finite element findings, approach those of third-order shear deformation theory for higher values of a/h. This means that with a decrease in overall plate thickness compared to its width a (thinner plate), FSDT becomes more applicable for prediction of $\bar{\tau}_{xz}$. Consequently, third-order shear deformation theory seems to be more appropriate for prediction of out-of-plane shear stress $\bar{\tau}_{xz}$ at lower values of a/*h* ratio. Figures 6 illustrates the distributions of peeling stress σ_z in the upper epoxy adhesive layer at *y*=b/2 based on h_1/h=0.1, h_2/h=0.02, h_3/h=0.76, a/*h*=20 and *n*=1. Second-order and third-order shear deformation theories are used to extract these results (Figs. 6(a)) and 6(b) respectively). According to both theories, the magnitudes of peeling stress σ_z appear to be constant along the adhesive layer thickness. Additionally, both theories predict the same amount of peeling stress for all values of *x* and *z*. According to Fig. 6(c), there is a close tie between finite element results and those of current solution based on first, second and third-order shear deformation theories.

Figures 7 shows the effect of any change in material parameter *n* and the adhesive thickness h_1 on non-dimensionalized planer stress $\bar{\sigma}_x$ in the epoxy adhesive layer. These results that are plotted along the adhesive thickness are based on the first, second and third-order shear deformation theories. The final element simulation findings are also superimposed for further comparison. The three foregoing theories seem to predict almost the same distributions along the thickness direction with a good accuracy. The maximum difference between finite element findings and those based on LT appears to be 9% (Fig. 7(a), *n*=0.5). For higher values of *n*, the percentage difference is decreased. According to Figs. 7(c) and 7(d), it is observed that any increase in thickness h_1 results in a decrease in planer stress $\bar{\sigma}_x$ in the adhesive layer. This variation along the adhesive thickness (h_2) seems to be linear. Fig. 7(d) indicates that the maximum difference between final element simulation results and those of LT that occurs at the adhesive-face sheet interface (z/h_2=0.5) is about 3%.

Based on the second-order shear deformation theory and *n*=1, the non-dimensional out-of-plane displacement $\bar{w}$ for the *x*-*y* plane located at *y*=b/2 in the core's mid-plane, is plotted in Fig. 8(a). Similar results based on other shear deformation theories and those of finite element findings are also shown for further comparison. Although LT seems to be able to predict this displacement component with a good accuracy, application of higher-order shear deformation theories does not seem to have a meaningful effect on these results.

4. Conclusions

In this study LT along with FSDT, SSDT, and TSDT were used to investigate the stress distribution in a five-layer sandwich plate subjected to a uniform distributed load. The aim of this study was to determine the applicability of LT along with the effect of other higher-order shear deformation theories on stress distribution in different layers of a simply supported composite sandwich plate. The effect of these theories on overall plate displacement was also studied. According to the results, for the assumed values of h_1, h_2, and h_3, the deduced values of displacement and planer stress, based on LT along with higher-order shear deformation theories (second and third), match those of FEA and FSDT. The accuracy of out-of-plane shear stress values

in the top face sheet along line 1 increases with implementation of higher-order shear deformation theories, although similar values at the core-adhesive and adhesive-cover sheet interface do not seem to be considerably improved. Higher values of a/*h* result in higher values of displacement, planer stress and out-of-plane shear stress, and their accuracy. The percentage differences between FE results and the three shear deformation theories seem to be reduced for higher values of a/*h* ratio (thinner composite plates), almost at all points introduced in this analysis. Additionally, SSDT and TSDT almost predict the same distribution for the two planer stress and out-of-plane shear stress components along the cover sheet thickness (as well as *x*-direction). Moreover, third-order shear deformation theory seems to be more appropriate for prediction of out-of-plane shear stress at lower values of a/*h* ratio. The results indicate that for the three shear deformation theories used in this analysis, the same distribution for out-of-plane shear stress is obtained in the core. The peak values of this stress occur at the plate edges.

According to the results, the magnitudes of peeling stress appear to be constant along the adhesive thickness. All three theories predict the same amount of peeling stress in the adhesive layer, at all values of *x* and *z*. Higher values of n result in higher values of planer stress in the core. Although LT along with FSDT seem to be well capable of predicting transverse displacement, application of higher-order shear deformation theories do not seem to have a meaningful effect on this component.

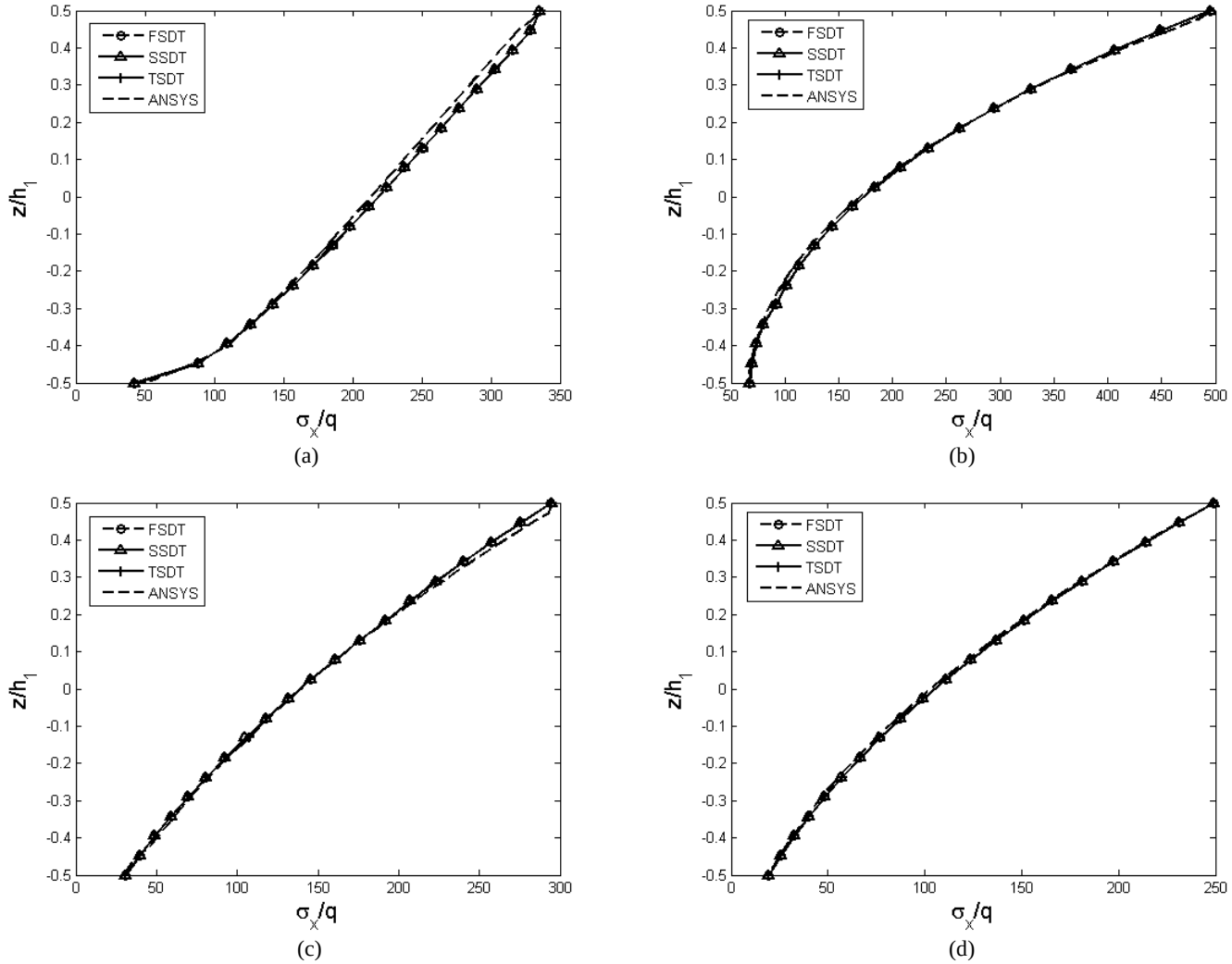

Fig. 3. Variations in $\bar{\sigma}_x$ along the cover sheet thickness on the line joining point 3 to 2 for a/*h*=20 . (a) *n*=0.5 , h_1/h=0.1 , (b) *n*=2, h_1/h=0.1 , (c) *n*=1, h_1/h=0.15 , (d) *n*=1, h_1/h=0.2 .

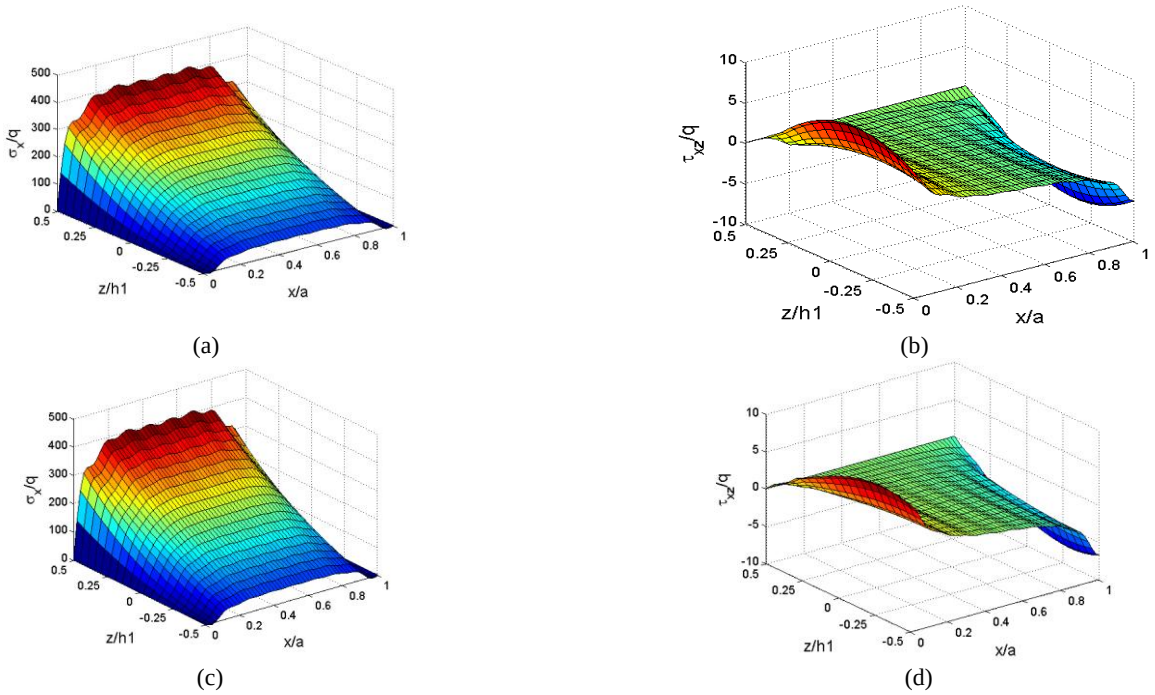

Fig. 4. Variations in $\bar{\sigma}_x$ and $\bar{\tau}_{xz}$ along x and z directions at y=b/2 in the top face sheet, based on h_1/h=0.1, h_2/h=0.02, h_3/h=0.76, a/h=20 and n=1 (a) LT along with SSDT (b) LT along with SSDT (c) LT along with TSDT (d) LT along with TSDT

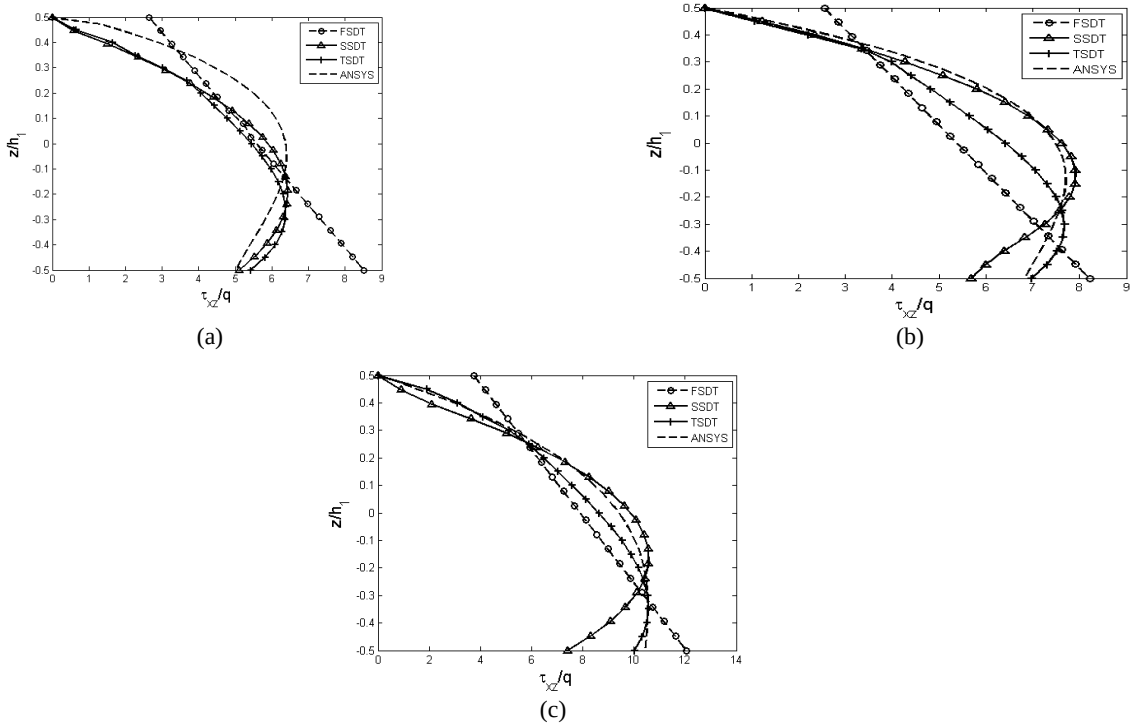

Fig. 5. Variations of $\bar{\tau}_{xz}$ along the thickness at line 1 (see Fig. 1) in the top face sheet for n=1, h_1/h=0.1, (a) a / h = 15, (b) a/h=20, (c) a / h = 30.

Table 4. Comparison of the results based on LT along with FSDT, SSDT and TSDT and those of FEA based on h_1/h=0.1, h_2/h=0.02, h_3/h=0.76, n=1.

$\frac{a}{h}$		$\bar{w}$	$\bar{\sigma}_x$					$\bar{\tau}_{xz}$			
		Point 1	Point 2	Point 3	Point 4	Point 5	Point 6	Max value on line 1	Point 7	Point 8	Point 9
15	FEA (ANSYS)	92.5988	224.5300	27.4050	1.7005	1.5445	0.87270	6.4038	5.0129	4.9987	4.9967
	LT FSDT	95.4725	234.5918	27.6297	1.6905	1.5667	0.82660	5.8674	5.0057	5.0057	4.9783
	% Difference	3.10	4.48	0.82	0.59	1.44	5.28	8.38	0.14	0.14	0.37
	LT SSDT	95.5060	234.7331	27.6859	1.6907	1.5669	0.82656	6.4372	5.0384	4.9680	4.9609
	% Difference	3.14	4.54	1.02	0.58	1.45	5.29	0.52	0.51	0.61	0.72
	LT TSDT	95.471	234.8117	27.5668	1.6895	1.5600	0.82692	6.3735	4.9507	4.9506	4.9481
	% Difference	3.10	4.58	0.59	0.65	1.00	5.25	0.47	1.24	0.96	0.97
20	FEA (ANSYS)	215.7120	388.8250	52.5050	3.3380	3.1130	1.6301	7.7091	6.8244	6.8177	6.8140
	LT FSDT	220.7483	388.790	51.8240	3.2365	3.0681	1.5016	5.6587	6.8113	6.8113	6.8238
	% Difference	2.33	0.01	1.30	3.04	1.44	7.88	26.60	0.19	0.09	0.14
	LT SSDT	220.8094	388.7977	51.8786	3.2366	3.0681	1.5017	7.9176	6.8441	6.7750	6.8244
	% Difference	2.36	0.01	1.19	3.04	1.44	7.88	2.70	0.29	0.63	0.15
	LT TSDT	220.7505	388.8012	51.7608	3.2366	3.0680	1.5016	7.6739	6.7639	6.7639	6.8044
	% Difference	2.34	0.01	1.42	3.04	1.45	7.88	0.46	0.89	0.79	0.11
30	FEA (ANSYS)	813.0153	855.2150	126.5600	7.0285	6.6055	3.4602	10.5540	10.4510	10.4410	10.4370
	LT FSDT	820.4410	855.2670	126.6997	6.9650	6.5362	3.4051	8.3057	10.4265	10.4265	10.2556
	% Difference	0.91	0.01	0.11	0.90	1.05	1.59	21.30	0.23	0.14	1.74
	LT SSDT	820.5762	855.2769	126.7558	6.9679	6.5388	3.4052	10.5759	10.4596	10.3928	10.2565
	% Difference	0.93	0.01	0.15	0.86	1.01	1.59	0.21	0.08	0.46	1.73
	LT TSDT	820.4448	855.2776	126.6426	6.9623	6.5300	3.4050	10.5732	10.3956	10.3956	10.3562
	% Difference	0.9138	0.01	0.07	0.94	1.14	1.60	0.18	0.53	0.43	0.77

Table 5. The effect of face sheet thickness on deflection $\bar{w}$ and stress components $\bar{\sigma}_x$, and $\bar{\tau}_{xz}$, based on FEA and LT for: a/h=20, h_2/h=0.02, n=1.

h_1/h		$\bar{w}$	$\bar{\sigma}_x$					$\bar{\tau}_{xz}$			
		Point 1	Point 2	Point 3	Point 4	Point 5	Point 6	Max value on line 1	Point 7	Point 8	Point 9
0.15	FEA	177.4287	294.9480	29.602	1.7740	1.5995	1.0008	7.9822	6.9192	6.9104	6.8878
	LT FSDT	180.5988	294.4104	30.7128	1.7528	1.6072	0.90290	8.1229	6.9400	6.9400	6.6493
	% Difference	1.79	0.18	3.75	1.20	0.4	9.78	1.76	0.30	0.43	3.46
	LT SSDT	180.6921	294.5030	30.7761	1.7564	1.6104	0.90292	7.9875	6.9878	6.8831	6.6491
	% Difference	1.84	0.15	3.97	0.99	0.68	9.78	0.07	0.99	0.40	3.47
	LT TSDT	180.5992	294.5304	30.6673	1.7502	1.6017	0.90304	7.9712	6.8941	6.8941	6.8122
	% Difference	1.79	0.14	3.60	1.34	0.14	9.77	0.14	0.36	0.24	1.10
0.2	FEA	153.5396	249.3700	19.1690	1.3070	1.1630	0.6275	8.3458	6.9669	6.9587	6.9579
	LT FSDT	155.8694	248.9687	19.3489	1.2643	1.1545	0.5651	8.4281	6.8280	6.8280	6.6915
	% Difference	1.52	0.16	0.94	3.27	0.73	9.94	0.99	1.99	1.88	3.83
	LT SSDT	156.0109	249.1642	19.3943	1.2646	1.1547	0.5652	8.3795	6.8652	6.7901	6.7080
	% Difference	1.61	0.08	1.18	3.24	0.71	9.93	0.40	1.46	2.42	3.59
	LT TSDT	155.8702	249.1770	19.3091	1.2647	1.1549	0.5653	8.3444	6.8120	6.8120	6.8544
	% Difference	1.52	0.08	0.73	3.24	0.70	9.91	0.02	2.22	2.11	1.49

Table 6. The effect of material parameter n on deflection $\bar{w}$ and stress components $\bar{\sigma}_x$, and $\bar{\tau}_{xz}$, based on FEA and LT for: h_1/h=0.1, h_2/h=0.02, h_3/h=0.76, a/h=20.

n		$\bar{w}$	$\bar{\sigma}_x$					$\bar{\tau}_{xz}$			
		Point 1	Point 2	Point 3	Point 4	Point 5	Point 6	Max value on line 1	Point 7	Point 8	Point 9
0.5	ANSYS	197.4901	335.02	41.210	2.5550	2.3555	1.3971	7.7714	6.8343	6.8312	6.8310
	LT FSDT	202.6148	335.4002	42.6457	2.4339	2.2583	1.2382	7.0634	6.7360	6.7360	6.5293
	% Difference	2.59	0.11	3.48	4.74	4.13	11.37	9.11	1.44	1.39	4.42
	LT SSDT	202.6481	335.4743	42.6719	2.4354	2.2596	1.2382	7.9129	6.7642	6.7061	6.5297
	% Difference	2.61	0.14	3.55	4.68	4.07	11.37	1.82	1.03	1.83	4.41
	LT TSDT	202.6148	335.5234	42.5990	2.4312	2.2503	1.2382	7.891	6.6957	6.6957	6.6448
	% Difference	2.59	0.15	3.37	4.85	4.47	11.37	1.54	2.03	1.98	2.73
2	ANSYS	246.5665	496.93	65.433	4.19	3.923	2.0275	7.4182	6.8117	6.8030	6.7977
	LT FSDT	250.2409	495.2669	67.0358	4.1405	3.9282	1.9226	7.4738	6.8668	6.8668	6.4667
	% Difference	1.49	0.33	2.45	1.18	0.13	5.17	0.75	0.81	0.94	4.87
	LT SSDT	250.5185	495.2457	67.1328	4.1403	3.9280	1.9225	7.4288	6.9035	6.8247	6.6182
	% Difference	1.60	0.34	2.60	1.19	0.13	5.18	0.14	1.35	0.32	2.64
	LT TSDT	250.2406	495.2871	66.9549	4.1405	3.9280	1.9225	7.4374	6.8137	6.8137	6.7478
	% Difference	1.49	0.33	2.33	1.18	0.13	5.18	0.26	0.03	0.16	0.73

Table 7. The geometric position of the points defined in Tables 4 to 6 with the coordinate system shown in Fig. 1.

Point's number	1	2	3	4	5	6	7	8	9
Location, on the	Core	Face sheet	Face sheet	adhesive	adhesive	Core	adhesive	adhesive	Core
x Coordinate	a/2	a/2	a/2	a/2	a/2	a/2	a/2	a/2	a/2
y Coordinate	b/2	b/2	b/2	b/2	b/2	b/2	0	0	0
z Coordinate	0	$h/2$	$h/2-h_1$	$h/2-h_1$	$h_3/2$	$h_3/2$	$h/2-h_1$	$h_3/2$	$h_3/2$

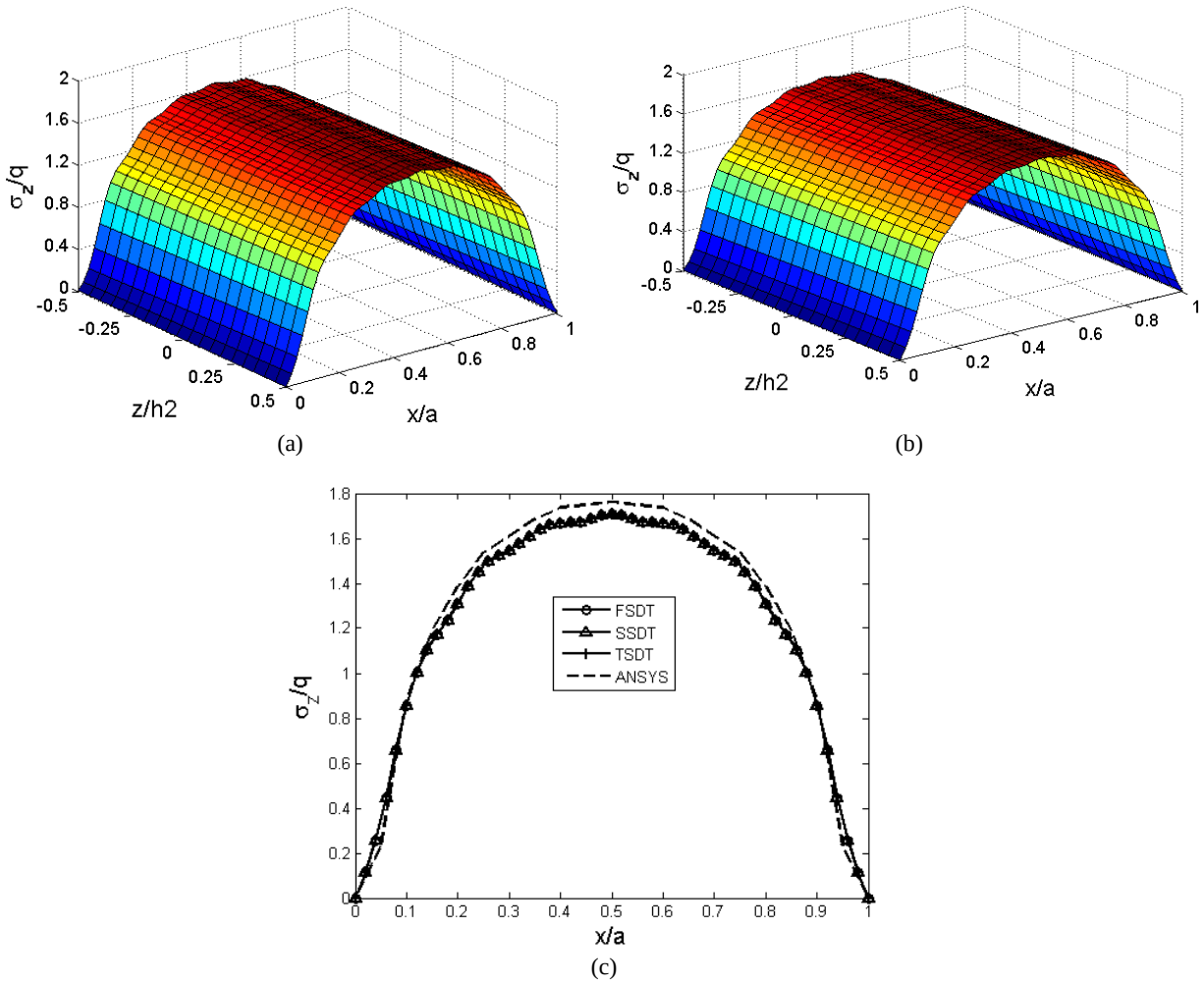

Fig. 6. Variations in $\bar{\sigma}_z$ in the top epoxy adhesive layer based on h_1/h=0.1, h_2/h=0.02, $h_3/h = 0.76$, $a/h = 20$ and n=1 at y=b/2 (a) LT along with SSDT (b) LT along with TSDT (c) At the adhesive-cover sheet interface.

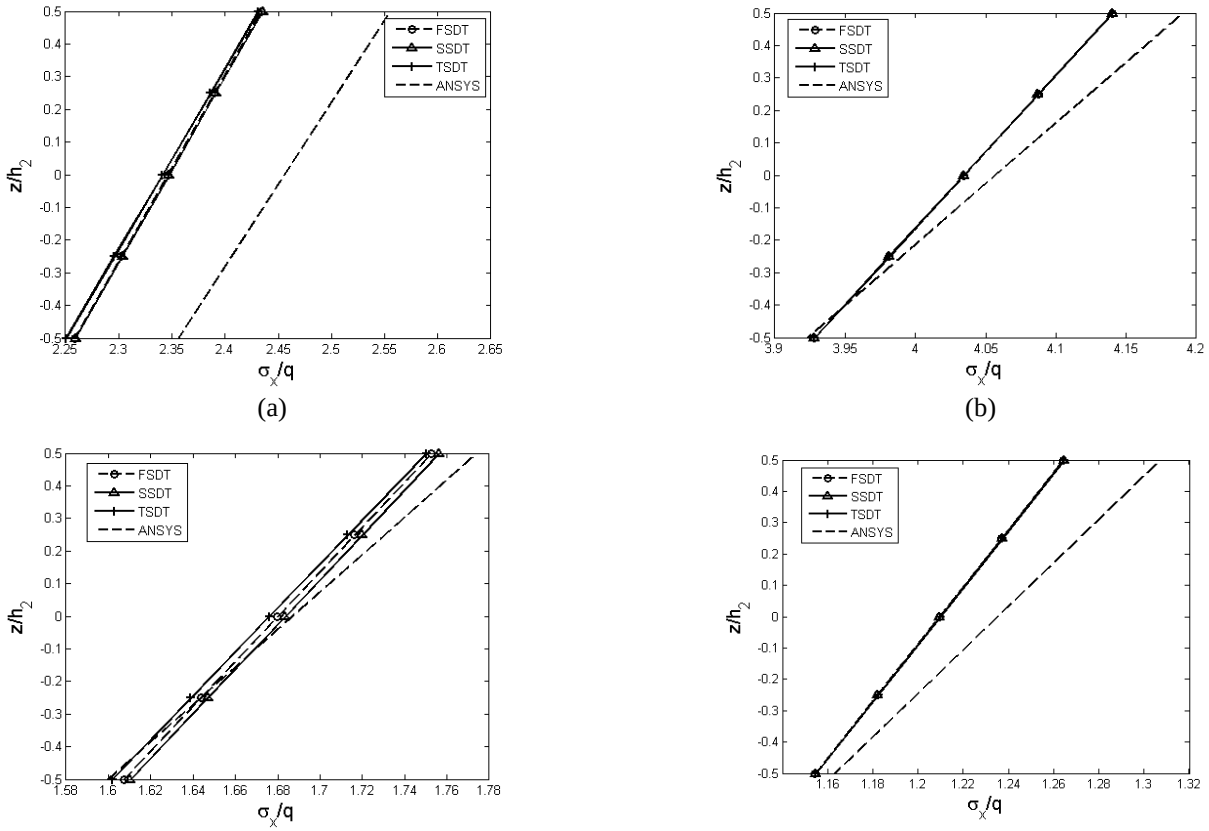

Fig. 7. Variations in $\bar{\sigma}_X$ in the top adhesive layer along the line joining point 5 to 4 (see Fig. 1) for a/h=20 , (a) n=0.5, h_1/h=0.1 , (b) n=2, h_1/h=0.1 , (c) n=1 , h_1/h=0.1 , (d) n=1 , h_1/h=0.2 .

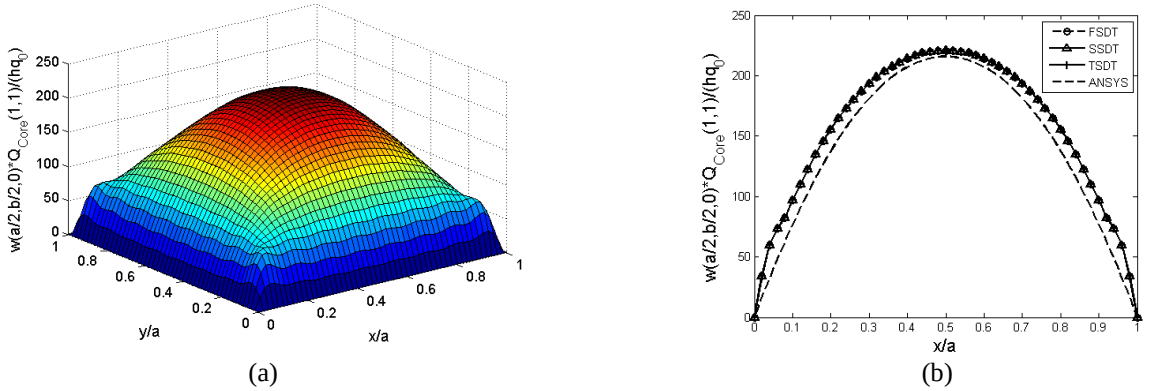

Fig. 8. Non-dimensional displacement $(\bar{w})$ in the core at y=b/2 based on h_1/h=0.1, h_2/h=0.02, h_3/h=0.76, a / h = 20 and n=1 (a) LT along with SSDT (b) LT along with FEA.

5. Appendix

Appendix *A*

Displacement components in a five-layer composite plate, based on the SSDT. z is measured from core mid-surface.

$$u^{(1)} = u - \frac{h_3}{2}\phi_x^{(3)} + \frac{h_3^2}{4}\psi_x^{(3)} - h_2\phi_x^{(2)} + \frac{h_2^2}{2}\psi_x^{(2)} - \frac{h_1}{2}\phi_x^{(1)} - \frac{h_1}{2}z^{(1)}\psi_x^{(1)} + z^{(1)}\phi_x^{(1)} + z^{(1)2}\psi_x^{(1)} \tag{A1}$$

$$v^{(1)} = v - \frac{h_3}{2}\phi_y^{(3)} + \frac{h_3^2}{4}\psi_y^{(3)} - h_2\phi_y^{(2)} + \frac{h_2^2}{2}\psi_y^{(2)} - \frac{h_1}{2}\phi_y^{(1)} - \frac{h_1}{2}z^{(1)}\psi_y^{(1)} + z^{(1)}\phi_y^{(1)} + z^{(1)2}\psi_y^{(1)} \tag{A2}$$

$$u^{(2)} = u - \frac{h_3}{2}\phi_x^{(3)} + \frac{h_3^2}{4}\psi_x^{(3)} - \frac{h_2}{2}\phi_x^{(2)} - \frac{h_2}{2}z^{(2)}\psi_x^{(2)} + z^{(2)}\phi_x^{(2)} + z^{(2)2}\psi_x^{(2)} \tag{A3}$$

$$v^{(2)} = v - \frac{h_3}{2}\phi_y^{(3)} + \frac{h_3^2}{4}\psi_y^{(3)} - \frac{h_2}{2}\phi_y^{(2)} - \frac{h_2}{2}z^{(2)}\psi_y^{(2)} + z^{(2)}\phi_y^{(2)} + z^{(2)2}\psi_y^{(2)} \tag{A4}$$

$$u^{(3)} = u + z^{(3)}\phi_x^{(3)} + z^{(3)2}\psi_x^{(3)}; v^{(3)} = v + z^{(3)}\phi_y^{(3)} + z^{(3)2}\psi_y^{(3)} \tag{A5}$$

$$u^{(4)} = u + \frac{h_3}{2}\phi_x^{(3)} + \frac{h_3^2}{4}\psi_x^{(3)} + \frac{h_2}{2}\phi_x^{(4)} + \frac{h_2}{2}z^{(4)}\psi_x^{(4)} + z^{(4)}\phi_x^{(4)} + z^{(4)2}\psi_x^{(4)} \tag{A6}$$

$$v^{(4)} = v + \frac{h_3}{2}\phi_y^{(3)} + \frac{h_3^2}{4}\psi_y^{(3)} + \frac{h_2}{2}\phi_y^{(4)} + \frac{h_2}{2}z^{(4)}\psi_y^{(4)} + z^{(4)}\phi_y^{(4)} + z^{(4)2}\psi_y^{(4)} \tag{A7}$$

$$u^{(5)} = u + \frac{h_3}{2}\phi_x^{(3)} + \frac{h_3^2}{4}\psi_x^{(3)} + h_2\phi_x^{(4)} + \frac{h_2^2}{2}\psi_x^{(4)} + \frac{h_1}{2}\phi_x^{(5)} + \frac{h_1}{2}z^{(5)}\psi_x^{(5)} + z^{(5)}\phi_x^{(5)} + z^{(5)2}\psi_x^{(5)} \tag{A8}$$

$$v^{(5)} = v + \frac{h_3}{2}\phi_y^{(3)} + \frac{h_3^2}{4}\psi_y^{(3)} + h_2\phi_y^{(4)} + \frac{h_2^2}{2}\psi_y^{(4)} + \frac{h_1}{2}\phi_y^{(5)} + \frac{h_1}{2}z^{(5)}\psi_y^{(5)} + z^{(5)}\phi_y^{(5)} + z^{(5)2}\psi_y^{(5)} \tag{A9}$$

$$w^{(1)} = w^{(2)} = w^{(3)} = w^{(4)} = w^{(5)} = w(x,y) \tag{A10}$$

In above equations $\phi_x^{(i)}(x,y)$, $\phi_y^{(i)}(x,y)$, $\psi_x^{(i)}(x,y)$ and $\psi_y^{(i)}(x,y)$ (i=1, 2, 3, 4, 5) are expressed in Eq. (7)

Appendix *B*

Displacement components in a five-layer composite plate, based on the TSDT. z is measured from core mid-surface.

$$u^{(1)} = u - \frac{h_3}{2}\phi_x^{(3)} - \frac{h_3^3}{8}\psi_x^{(3)} - h_2\phi_x^{(2)} - \frac{h_2^3}{4}\psi_x^{(2)} - \frac{h_1}{2}\phi_x^{(1)} - \frac{h_1^3}{8}\psi_x^{(1)} + z^{(1)}\phi_x^{(1)} + z^{(1)3}\psi_x^{(1)} \tag{B1}$$

$$v^{(1)} = v - \frac{h_3}{2}\phi_y^{(3)} - \frac{h_3^3}{8}\psi_y^{(3)} - h_2\phi_y^{(2)} - \frac{h_2^3}{4}\psi_y^{(2)} - \frac{h_1}{2}\phi_y^{(1)} - \frac{h_1^3}{8}\psi_y^{(1)} + z^{(1)}\phi_y^{(1)} + z^{(1)3}\psi_y^{(1)} \tag{B2}$$

$$u^{(2)} = u - \frac{h_3}{2}\phi_x^{(3)} - \frac{h_3^3}{8}\psi_x^{(3)} - \frac{h_2}{2}\phi_x^{(2)} - \frac{h_2^3}{8}\psi_x^{(2)} + z^{(2)}\phi_x^{(2)} + z^{(2)3}\psi_x^{(2)} \tag{B3}$$

$$v^{(2)} = v - \frac{h_3}{2}\phi_y^{(3)} - \frac{h_3^3}{8}\psi_y^{(3)} - \frac{h_2}{2}\phi_y^{(2)} - \frac{h_2^3}{8}\psi_y^{(2)} + z^{(2)}\phi_y^{(2)} + z^{(2)3}\psi_y^{(2)} \tag{B4}$$

$$u^{(3)} = u + z^{(3)}\phi_x^{(3)} + z^{(3)3}\psi_x^{(3)}; v^{(3)} = v + z^{(3)}\phi_y^{(3)} + z^{(3)3}\psi_y^{(3)} \tag{B5}$$

$$u^{(4)} = u + \frac{h_3}{2}\phi_x^{(3)} + \frac{h_3^3}{8}\psi_x^{(3)} + \frac{h_2}{2}\phi_x^{(4)} + \frac{h_2^3}{8}\psi_x^{(4)} + z^{(4)}\phi_x^{(4)} + z^{(4)3}\psi_x^{(4)} \tag{B6}$$

$$v^{(4)} = v + \frac{h_3}{2}\phi_y^{(3)} + \frac{h_3^3}{8}\psi_y^{(3)} + \frac{h_2}{2}\phi_y^{(4)} + \frac{h_2^3}{8}\psi_y^{(4)} + z^{(4)}\phi_y^{(4)} + z^{(4)3}\psi_y^{(4)} \tag{B7}$$

$$u^{(5)} = u + \frac{h_3}{2}\phi_x^{(3)} + \frac{h_3^3}{8}\psi_x^{(3)} + h_2\phi_x^{(4)} + \frac{h_2^3}{4}\psi_x^{(4)} + \frac{h_1}{2}\phi_x^{(5)} + \frac{h_1^3}{8}\psi_x^{(5)} + z^{(5)}\phi_x^{(5)} + z^{(5)3}\psi_x^{(5)} \tag{B8}$$

$$v^{(5)} = v + \frac{h_3}{2}\phi_y^{(3)} + \frac{h_3^3}{8}\psi_y^{(3)} + h_2\phi_y^{(4)} + \frac{h_2^3}{4}\psi_y^{(4)} + \frac{h_1}{2}\phi_y^{(5)} + \frac{h_1^3}{8}\psi_y^{(5)} + z^{(5)}\phi_y^{(5)} + z^{(5)3}\psi_y^{(5)} \tag{B9}$$

$$w^{(1)} = w^{(2)} = w^{(3)} = w^{(4)} = w^{(5)} = w(x,y) \tag{B10}$$

In above equations $\phi_x^{(i)}(x,y)$, $\phi_y^{(i)}(x,y)$, $\psi_x^{(i)}(x,y)$ and $\psi_y^{(i)}(x,y)$ (i=1, 2, 3, 4, 5) are expressed in Eq. (7)

Appendix *C*

The governing equations of equilibrium in a five-layer sandwich composite plate using LT and SSDT.

$$\sum_{k=1}^{5}\left(\frac{\partial N_1^{(k)}}{\partial x} + \frac{\partial N_6^{(k)}}{\partial y}\right) = 0; \sum_{k=1}^{5}\left(\frac{\partial N_2^{(k)}}{\partial y} + \frac{\partial N_6^{(k)}}{\partial x}\right) = 0; \sum_{k=1}^{5}\left(\frac{\partial Q_1^{(k)}}{\partial x} + \frac{\partial Q_2^{(k)}}{\partial y}\right) - q = 0 \tag{C1}$$

$$-\frac{h_1}{2}\left(\frac{\partial N_1^{(1)}}{\partial x} + \frac{\partial N_6^{(1)}}{\partial y}\right) + Q_1^{(1)} - \frac{\partial M_6^{(1)}}{\partial y} - \frac{\partial M_1^{(1)}}{\partial x} = 0; -\frac{h_1}{2}\left(\frac{\partial N_2^{(1)}}{\partial y} + \frac{\partial N_6^{(1)}}{\partial x}\right) + Q_2^{(1)} - \frac{\partial M_6^{(1)}}{\partial x} - \frac{\partial M_2^{(1)}}{\partial y} = 0 \tag{C2}$$

$$h_2\left(\frac{\partial N_1^{(1)}}{\partial x}+\frac{\partial N_6^{(1)}}{\partial y}\right)-\frac{h_2}{2}\left(\frac{\partial N_1^{(2)}}{\partial x}+\frac{\partial N_6^{(2)}}{\partial y}\right)+Q_1^{(2)}-\frac{\partial M_1^{(2)}}{\partial x}-\frac{\partial M_6^{(2)}}{\partial y}=0 \tag{C3}$$

$$h_2\left(\frac{\partial N_2^{(1)}}{\partial y}+\frac{\partial N_6^{(1)}}{\partial x}\right)-\frac{h_2}{2}\left(\frac{\partial N_2^{(2)}}{\partial y}+\frac{\partial N_6^{(2)}}{\partial x}\right)+Q_2^{(2)}-\frac{\partial M_2^{(2)}}{\partial y}-\frac{\partial M_6^{(2)}}{\partial x}=0 \tag{C4}$$

$$\frac{h_3}{2}\left(\frac{\partial N_1^{(1)}}{\partial x}+\frac{\partial N_6^{(1)}}{\partial y}+\frac{\partial N_1^{(2)}}{\partial x}+\frac{\partial N_6^{(2)}}{\partial y}-\frac{\partial N_1^{(4)}}{\partial x}-\frac{\partial N_6^{(4)}}{\partial y}-\frac{\partial N_1^{(5)}}{\partial x}-\frac{\partial N_6^{(5)}}{\partial y}\right)+Q_1^{(3)}-\frac{\partial M_1^{(3)}}{\partial x}-\frac{\partial M_6^{(3)}}{\partial y}=0 \tag{C5}$$

$$\frac{h_3}{2}\left(\frac{\partial N_2^{(1)}}{\partial y}+\frac{\partial N_6^{(1)}}{\partial x}+\frac{\partial N_2^{(2)}}{\partial y}+\frac{\partial N_6^{(2)}}{\partial x}-\frac{\partial N_2^{(4)}}{\partial y}-\frac{\partial N_6^{(4)}}{\partial x}-\frac{\partial N_2^{(5)}}{\partial y}-\frac{\partial N_6^{(5)}}{\partial x}\right)+Q_2^{(3)}-\frac{\partial M_2^{(3)}}{\partial y}-\frac{\partial M_6^{(3)}}{\partial x}=0 \tag{C6}$$

$$-h_2\left(\frac{\partial N_1^{(5)}}{\partial x}+\frac{\partial N_6^{(5)}}{\partial y}\right)+\frac{h_2}{2}\left(\frac{\partial N_1^{(4)}}{\partial x}+\frac{\partial N_6^{(4)}}{\partial y}\right)+Q_1^{(4)}-\frac{\partial M_1^{(4)}}{\partial x}-\frac{\partial M_6^{(4)}}{\partial y}=0 \tag{C7}$$

$$-h_2\left(\frac{\partial N_2^{(5)}}{\partial y}+\frac{\partial N_6^{(5)}}{\partial x}\right)+\frac{h_2}{2}\left(\frac{\partial N_2^{(4)}}{\partial y}+\frac{\partial N_6^{(4)}}{\partial x}\right)+Q_2^{(4)}-\frac{\partial M_2^{(4)}}{\partial y}-\frac{\partial M_6^{(4)}}{\partial x}=0 \tag{C8}$$

$$\frac{h_1}{2}\left(\frac{\partial N_1^{(5)}}{\partial x}+\frac{\partial N_6^{(5)}}{\partial y}\right)+Q_1^{(5)}-\frac{\partial M_6^{(5)}}{\partial y}-\frac{\partial M_1^{(5)}}{\partial x}=0;\ \frac{h_1}{2}\left(\frac{\partial N_2^{(5)}}{\partial y}+\frac{\partial N_6^{(5)}}{\partial x}\right)+Q_2^{(5)}-\frac{\partial M_6^{(5)}}{\partial x}-\frac{\partial M_2^{(5)}}{\partial y}=0 \tag{C9}$$

$$\frac{h_1}{2}\left(\frac{\partial M_1^{(1)}}{\partial x}+\frac{\partial M_6^{(1)}}{\partial y}\right)-\frac{h_1}{2}Q_1^{(1)}-2R_1^{(1)}+\frac{\partial L_1^{(1)}}{\partial x}+\frac{\partial L_6^{(1)}}{\partial y}=0;\ \frac{h_1}{2}\left(\frac{\partial M_2^{(1)}}{\partial y}+\frac{\partial M_6^{(1)}}{\partial x}\right)-\frac{h_1}{2}Q_2^{(1)}-2R_2^{(1)}+\frac{\partial L_2^{(1)}}{\partial y}+\frac{\partial L_6^{(1)}}{\partial x}=0 \tag{C10}$$

$$-\frac{h_2^2}{2}\left(\frac{\partial N_1^{(1)}}{\partial x}+\frac{\partial N_6^{(1)}}{\partial y}\right)+\frac{h_2}{2}\left(\frac{\partial M_1^{(2)}}{\partial x}+\frac{\partial M_6^{(2)}}{\partial y}\right)-\frac{h_2}{2}Q_1^{(2)}-2R_1^{(2)}+\frac{\partial L_1^{(2)}}{\partial x}+\frac{\partial L_6^{(2)}}{\partial y}=0 \tag{C11}$$

$$-\frac{h_2^2}{2}\left(\frac{\partial N_2^{(1)}}{\partial y}+\frac{\partial N_6^{(1)}}{\partial x}\right)+\frac{h_2}{2}\left(\frac{\partial M_2^{(2)}}{\partial y}+\frac{\partial M_6^{(2)}}{\partial x}\right)-\frac{h_2}{2}Q_2^{(2)}-2R_2^{(2)}+\frac{\partial L_2^{(2)}}{\partial y}+\frac{\partial L_6^{(2)}}{\partial x}=0 \tag{C12}$$

$$-\frac{h_3^2}{4}\left(\frac{\partial N_1^{(1)}}{\partial x}+\frac{\partial N_6^{(1)}}{\partial y}+\frac{\partial N_1^{(2)}}{\partial x}+\frac{\partial N_6^{(2)}}{\partial y}+\frac{\partial N_1^{(4)}}{\partial x}+\frac{\partial N_6^{(4)}}{\partial y}+\frac{\partial N_1^{(5)}}{\partial x}+\frac{\partial N_6^{(5)}}{\partial y}\right)-2R_1^{(3)}+\frac{\partial L_1^{(3)}}{\partial x}+\frac{\partial L_6^{(3)}}{\partial y}=0 \tag{C13}$$

$$-\frac{h_3^2}{4}\left(\frac{\partial N_2^{(1)}}{\partial y}+\frac{\partial N_6^{(1)}}{\partial x}+\frac{\partial N_2^{(2)}}{\partial y}+\frac{\partial N_6^{(2)}}{\partial x}+\frac{\partial N_2^{(4)}}{\partial y}+\frac{\partial N_6^{(4)}}{\partial x}+\frac{\partial N_2^{(5)}}{\partial y}+\frac{\partial N_6^{(5)}}{\partial x}\right)-2R_2^{(3)}+\frac{\partial L_2^{(3)}}{\partial y}+\frac{\partial L_6^{(3)}}{\partial x}=0 \tag{C14}$$

$$-\frac{h_2^2}{2}\left(\frac{\partial N_1^{(5)}}{\partial x}+\frac{\partial N_6^{(5)}}{\partial y}\right)-\frac{h_2}{2}\left(\frac{\partial M_1^{(4)}}{\partial x}+\frac{\partial M_6^{(4)}}{\partial y}\right)+\frac{h_2}{2}Q_1^{(4)}-2R_1^{(4)}+\frac{\partial L_1^{(4)}}{\partial x}+\frac{\partial L_6^{(4)}}{\partial y}=0 \tag{C15}$$

$$-\frac{h_2^2}{2}\left(\frac{\partial N_2^{(5)}}{\partial y}+\frac{\partial N_6^{(5)}}{\partial x}\right)-\frac{h_2}{2}\left(\frac{\partial M_2^{(4)}}{\partial y}+\frac{\partial M_6^{(4)}}{\partial x}\right)+\frac{h_2}{2}Q_2^{(4)}-2R_2^{(4)}+\frac{\partial L_2^{(4)}}{\partial y}+\frac{\partial L_6^{(4)}}{\partial x}=0 \tag{C16}$$

$$-\frac{h_1}{2}\left(\frac{\partial M_1^{(5)}}{\partial x}+\frac{\partial M_6^{(5)}}{\partial y}\right)+\frac{h_1}{2}Q_1^{(5)}-2R_1^{(5)}+\frac{\partial L_1^{(5)}}{\partial x}+\frac{\partial L_6^{(5)}}{\partial y}=0;\ -\frac{h_1}{2}\left(\frac{\partial M_2^{(5)}}{\partial y}+\frac{\partial M_6^{(5)}}{\partial x}\right)+\frac{h_1}{2}Q_2^{(5)}-2R_2^{(5)}+\frac{\partial L_2^{(5)}}{\partial y}+\frac{\partial L_6^{(5)}}{\partial x}=0 \tag{C17}$$

In above equations, parameters $N_i^{(k)}$, $M_i^{(k)}$ and $L_i^{(k)}$ (i=1, 2, 6), $Q_j^{(k)}$ and $R_j^{(k)}$ (j=1, 2), (k=1, 2, 3, 4, 5) are expressed in Appendix *E* (Eqs. (E1)).

Appendix *D*

The governing equations of equilibrium in a five-layer sandwich composite plate using LT and TSDT.

$$\sum_{k=1}^{5}\left(\frac{\partial N_1^{(k)}}{\partial x}+\frac{\partial N_6^{(k)}}{\partial y}\right)=0;\ \sum_{k=1}^{5}\left(\frac{\partial N_2^{(k)}}{\partial y}+\frac{\partial N_6^{(k)}}{\partial x}\right)=0;\ \sum_{k=1}^{5}\left(\frac{\partial Q_1^{(k)}}{\partial x}+\frac{\partial Q_2^{(k)}}{\partial y}\right)-q=0 \tag{D1}$$

$$-\frac{h_1}{2}\left(\frac{\partial N_1^{(1)}}{\partial x}+\frac{\partial N_6^{(1)}}{\partial y}\right)+Q_1^{(1)}-\frac{\partial M_6^{(1)}}{\partial y}-\frac{\partial M_1^{(1)}}{\partial x}=0;-\frac{h_1}{2}\left(\frac{\partial N_2^{(1)}}{\partial y}+\frac{\partial N_6^{(1)}}{\partial x}\right)+Q_2^{(1)}-\frac{\partial M_6^{(1)}}{\partial x}-\frac{\partial M_2^{(1)}}{\partial y}=0 \tag{D2}$$

$$h_2\left(\frac{\partial N_1^{(1)}}{\partial x}+\frac{\partial N_6^{(1)}}{\partial y}\right)-\frac{h_2}{2}\left(\frac{\partial N_1^{(2)}}{\partial x}+\frac{\partial N_6^{(2)}}{\partial y}\right)+Q_1^{(2)}-\frac{\partial M_1^{(2)}}{\partial x}-\frac{\partial M_6^{(2)}}{\partial y}=0 \tag{D3}$$

$$h_2\left(\frac{\partial N_2^{(1)}}{\partial y}+\frac{\partial N_6^{(1)}}{\partial x}\right)-\frac{h_2}{2}\left(\frac{\partial N_2^{(2)}}{\partial y}+\frac{\partial N_6^{(2)}}{\partial x}\right)+Q_2^{(2)}-\frac{\partial M_2^{(2)}}{\partial y}-\frac{\partial M_6^{(2)}}{\partial x}=0 \tag{D4}$$

$$\frac{h_3}{2}\left(\frac{\partial N_1^{(1)}}{\partial x}+\frac{\partial N_6^{(1)}}{\partial y}+\frac{\partial N_1^{(2)}}{\partial x}+\frac{\partial N_6^{(2)}}{\partial y}-\frac{\partial N_1^{(4)}}{\partial x}-\frac{\partial N_6^{(4)}}{\partial y}-\frac{\partial N_1^{(5)}}{\partial x}-\frac{\partial N_6^{(5)}}{\partial y}\right)+Q_1^{(3)}-\frac{\partial M_1^{(3)}}{\partial x}-\frac{\partial M_6^{(3)}}{\partial y}=0 \tag{D5}$$

$$\frac{h_3}{2}\left(\frac{\partial N_2^{(1)}}{\partial y}+\frac{\partial N_6^{(1)}}{\partial x}+\frac{\partial N_2^{(2)}}{\partial y}+\frac{\partial N_6^{(2)}}{\partial x}-\frac{\partial N_2^{(4)}}{\partial y}-\frac{\partial N_6^{(4)}}{\partial x}-\frac{\partial N_2^{(5)}}{\partial y}-\frac{\partial N_6^{(5)}}{\partial x}\right)+Q_2^{(3)}-\frac{\partial M_2^{(3)}}{\partial y}-\frac{\partial M_6^{(3)}}{\partial x}=0 \tag{D6}$$

$$-h_2\left(\frac{\partial N_1^{(5)}}{\partial x}+\frac{\partial N_6^{(5)}}{\partial y}\right)+\frac{h_2}{2}\left(\frac{\partial N_1^{(4)}}{\partial x}+\frac{\partial N_6^{(4)}}{\partial y}\right)+Q_1^{(4)}-\frac{\partial M_1^{(4)}}{\partial x}-\frac{\partial M_6^{(4)}}{\partial y}=0 \tag{D7}$$

$$-h_2\left(\frac{\partial N_2^{(5)}}{\partial y}+\frac{\partial N_6^{(5)}}{\partial x}\right)+\frac{h_2}{2}\left(\frac{\partial N_2^{(4)}}{\partial y}+\frac{\partial N_6^{(4)}}{\partial x}\right)+Q_2^{(4)}-\frac{\partial M_2^{(4)}}{\partial y}-\frac{\partial M_6^{(4)}}{\partial x}=0 \tag{D8}$$

$$\frac{h_1}{2}\left(\frac{\partial N_1^{(5)}}{\partial x}+\frac{\partial N_6^{(5)}}{\partial y}\right)+Q_1^{(5)}-\frac{\partial M_6^{(5)}}{\partial y}-\frac{\partial M_1^{(5)}}{\partial x}=0;\ \frac{h_1}{2}\left(\frac{\partial N_2^{(5)}}{\partial y}+\frac{\partial N_6^{(5)}}{\partial x}\right)+Q_2^{(5)}-\frac{\partial M_6^{(5)}}{\partial x}-\frac{\partial M_2^{(5)}}{\partial y}=0 \tag{D9}$$

$$-\frac{h_1^3}{8}\left(\frac{\partial N_1^{(1)}}{\partial x}+\frac{\partial N_6^{(1)}}{\partial y}\right)+3K_1^{(1)}-\frac{\partial P_1^{(1)}}{\partial x}-\frac{\partial P_6^{(1)}}{\partial y}=0;-\frac{h_1^3}{8}\left(\frac{\partial N_2^{(1)}}{\partial y}+\frac{\partial N_6^{(1)}}{\partial x}\right)+3K_2^{(1)}-\frac{\partial P_2^{(1)}}{\partial y}-\frac{\partial P_6^{(1)}}{\partial x}=0 \tag{D10}$$

$$\frac{h_2^3}{4}\left(\frac{\partial N_1^{(1)}}{\partial x}+\frac{\partial N_6^{(1)}}{\partial y}\right)-\frac{h_2^3}{8}\left(\frac{\partial N_1^{(2)}}{\partial x}+\frac{\partial N_6^{(2)}}{\partial y}\right)+3K_1^{(2)}-\frac{\partial P_1^{(2)}}{\partial x}-\frac{\partial P_6^{(2)}}{\partial y}=0 \tag{D11}$$

$$\frac{h_2^3}{4}\left(\frac{\partial N_2^{(1)}}{\partial y}+\frac{\partial N_6^{(1)}}{\partial x}\right)-\frac{h_2^3}{8}\left(\frac{\partial N_2^{(2)}}{\partial y}+\frac{\partial N_6^{(2)}}{\partial x}\right)+3K_2^{(2)}-\frac{\partial P_2^{(2)}}{\partial y}-\frac{\partial P_6^{(2)}}{\partial x}=0 \tag{D12}$$

$$\frac{h_3^3}{8}\left(\frac{\partial N_1^{(1)}}{\partial x}+\frac{\partial N_6^{(1)}}{\partial y}+\frac{\partial N_1^{(2)}}{\partial x}+\frac{\partial N_6^{(2)}}{\partial y}-\frac{\partial N_1^{(4)}}{\partial x}-\frac{\partial N_6^{(4)}}{\partial y}-\frac{\partial N_1^{(5)}}{\partial x}-\frac{\partial N_6^{(5)}}{\partial y}\right)+3K_1^{(3)}-\frac{\partial P_1^{(3)}}{\partial x}-\frac{\partial P_6^{(3)}}{\partial y}=0 \tag{D13}$$

$$\frac{h_3^3}{8}\left(\frac{\partial N_2^{(1)}}{\partial y}+\frac{\partial N_6^{(1)}}{\partial x}+\frac{\partial N_2^{(2)}}{\partial y}+\frac{\partial N_6^{(2)}}{\partial x}-\frac{\partial N_2^{(4)}}{\partial y}-\frac{\partial N_6^{(4)}}{\partial x}-\frac{\partial N_2^{(5)}}{\partial y}-\frac{\partial N_6^{(5)}}{\partial x}\right)+3K_2^{(3)}-\frac{\partial P_2^{(3)}}{\partial y}-\frac{\partial P_6^{(3)}}{\partial x}=0 \tag{D14}$$

$$-\frac{h_2^3}{4}\left(\frac{\partial N_1^{(5)}}{\partial x}+\frac{\partial N_6^{(5)}}{\partial y}\right)+\frac{h_2^3}{8}\left(\frac{\partial N_1^{(4)}}{\partial x}+\frac{\partial N_6^{(4)}}{\partial y}\right)+3K_1^{(4)}-\frac{\partial P_1^{(4)}}{\partial x}-\frac{\partial P_6^{(4)}}{\partial y}=0 \tag{D15}$$

$$-\frac{h_2^3}{4}\left(\frac{\partial N_2^{(5)}}{\partial y}+\frac{\partial N_6^{(5)}}{\partial x}\right)+\frac{h_2^3}{8}\left(\frac{\partial N_2^{(4)}}{\partial y}+\frac{\partial N_6^{(4)}}{\partial x}\right)+3K_2^{(4)}-\frac{\partial P_2^{(4)}}{\partial y}-\frac{\partial P_6^{(4)}}{\partial x}=0 \tag{D16}$$

$$\frac{h_1^3}{8}\left(\frac{\partial N_1^{(5)}}{\partial x}+\frac{\partial N_6^{(5)}}{\partial y}\right)+3K_1^{(5)}-\frac{\partial P_1^{(5)}}{\partial x}-\frac{\partial P_6^{(5)}}{\partial y}=0;\ \frac{h_1^3}{8}\left(\frac{\partial N_2^{(5)}}{\partial y}+\frac{\partial N_6^{(5)}}{\partial x}\right)+3K_2^{(5)}-\frac{\partial P_2^{(5)}}{\partial y}-\frac{\partial P_6^{(5)}}{\partial x}=0 \tag{D17}$$

In above equations, parameters $N_i^{(k)}$, $M_i^{(k)}$ and $P_i^{(k)}$ (i=1, 2, 6), $Q_j^{(k)}$ and $K_j^{(k)}$ (j=1, 2), (k=1, 2, 3, 4, 5) are expressed in Appendix *E* (Eqs. (E2)).

Appendix *E*

Definition of parameters $N_i^{(k)}$, $M_i^{(k)}$ and $L_i^{(k)}$ (i=1, 2, 6), $Q_j^{(k)}$ and $R_j^{(k)}$ (j=1, 2), (k=1, 2, 3, 4, 5) used in the governing equations of equilibrium presented in Appendix *C* for a five-layer sandwich composite plate using LT and SSDT.

$$\begin{bmatrix} N_1^{(k)} \\ N_2^{(k)} \\ N_6^{(k)} \\ M_1^{(k)} \\ M_2^{(k)} \\ M_6^{(k)} \\ L_1^{(k)} \\ L_2^{(k)} \\ L_6^{(k)} \end{bmatrix} = \begin{bmatrix} [A]^{(k)} & [B]^{(k)} & [D]^{(k)} \\ [B]^{(k)} & [D]^{(k)} & [E]^{(k)} \\ [D]^{(k)} & [E]^{(k)} & [F]^{(k)} \end{bmatrix} \begin{bmatrix} \varepsilon_x^{0(k)} \\ \varepsilon_y^{0(k)} \\ \gamma_{xy}^{0(k)} \\ \varepsilon_x^{1(k)} \\ \varepsilon_y^{1(k)} \\ \gamma_{xy}^{1(k)} \\ \varepsilon_x^{2(k)} \\ \varepsilon_y^{2(k)} \\ \gamma_{xy}^{2(k)} \end{bmatrix}; \begin{bmatrix} Q_1^{(k)} \\ Q_2^{(k)} \\ R_1^{(k)} \\ R_2^{(k)} \end{bmatrix} = \begin{bmatrix} A_{55}^{(k)} & A_{54}^{(k)} & B_{55}^{(k)} & B_{54}^{(k)} \\ A_{45}^{(k)} & A_{44}^{(k)} & B_{45}^{(k)} & B_{44}^{(k)} \\ B_{55}^{(k)} & B_{54}^{(k)} & D_{55}^{(k)} & D_{54}^{(k)} \\ B_{45}^{(k)} & B_{44}^{(k)} & D_{45}^{(k)} & D_{44}^{(k)} \end{bmatrix} \begin{bmatrix} \gamma_{xz}^{0(k)} \\ \gamma_{yz}^{0(k)} \\ \gamma_{xz}^{1(k)} \\ \gamma_{yz}^{1(k)} \end{bmatrix} \tag{E1}$$

Definition of parameters $N_i^{(k)}$, $M_i^{(k)}$ and $P_i^{(k)}$ (i=1, 2, 6), $Q_j^{(k)}$ and $K_j^{(k)}$ (j=1, 2), (k=1, 2, 3, 4, 5) used in the governing equations of equilibrium presented in Appendix *D* for a five-layer sandwich composite plate using LT and TSDT.

$$\begin{bmatrix} N_1^{(k)} \\ N_2^{(k)} \\ N_6^{(k)} \\ M_1^{(k)} \\ M_2^{(k)} \\ M_6^{(k)} \\ P_1^{(k)} \\ P_2^{(k)} \\ P_6^{(k)} \end{bmatrix} = \begin{bmatrix} [A]^{(k)} & [B]^{(k)} & [E]^{(k)} \\ [B]^{(k)} & [D]^{(k)} & [F]^{(k)} \\ [E]^{(k)} & [F]^{(k)} & [H]^{(k)} \end{bmatrix} \begin{bmatrix} \varepsilon_x^{0(k)} \\ \varepsilon_y^{0(k)} \\ \gamma_{xy}^{0(k)} \\ \varepsilon_x^{1(k)} \\ \varepsilon_y^{1(k)} \\ \gamma_{xy}^{1(k)} \\ \varepsilon_x^{3(k)} \\ \varepsilon_y^{3(k)} \\ \gamma_{xy}^{3(k)} \end{bmatrix}; \begin{bmatrix} Q_1^{(k)} \\ Q_2^{(k)} \\ K_1^{(k)} \\ K_2^{(k)} \end{bmatrix} = \begin{bmatrix} A_{55}^{(k)} & A_{54}^{(k)} & J_{55}^{(k)} & J_{54}^{(k)} \\ A_{45}^{(k)} & A_{44}^{(k)} & J_{45}^{(k)} & J_{44}^{(k)} \\ J_{55}^{(k)} & J_{54}^{(k)} & L_{55}^{(k)} & L_{54}^{(k)} \\ J_{45}^{(k)} & J_{44}^{(k)} & L_{45}^{(k)} & L_{44}^{(k)} \end{bmatrix} \begin{bmatrix} \gamma_{xz}^{0(k)} \\ \gamma_{yz}^{0(k)} \\ \gamma_{xz}^{2(k)} \\ \gamma_{yz}^{2(k)} \end{bmatrix} \tag{E2}$$

The elements of matrices *A*, *B*, *D*, *E*, *F*, *H*, *J* and *L*, (k=1, 2, 3, 4, 5) are given in Eqs. (E3) and (E4).

$$\left(A_{ij}^{(k)}, B_{ij}^{(k)}, D_{ij}^{(k)}, E_{ij}^{(k)}, F_{ij}^{(k)}, H_{ij}^{(k)}\right) = \int_{-\frac{h_k}{2}}^{\frac{h_k}{2}} Q_{ij}^{(k)} \left(1, z, z^2, z^3, z^4, z^6\right) dz \qquad i = 1,2,6 \tag{E3}$$

$$\left(A_{ij}^{(k)}, B_{ij}^{(k)}, D_{ij}^{(k)}, J_{ij}^{(k)}, L_{ij}^{(k)}\right) = \int_{-\frac{h_k}{2}}^{\frac{h_k}{2}} Q_{ij}^{(k)} \left(1, z, z^2, z^2, z^4\right) dz \qquad i = 4,5 \tag{E4}$$

Where for the materials in Table 3, $Q_{ij}^{(k)} = 0, \text{ for } (i \neq j), i = 4,5$

6. References

[1] B. Liu., A. J. M. Ferreira, Y. F. Xing, A. M. A. Neves, Analysis of composite plates using a layerwise theory and a differential quadrature finite element method, *Composite Structures* Vol. 156, pp. 6, 2016.

[2] M. E. Fares, M. K. H. Elmarghany, M. G. Salem, A layerwise theory for Nth-layer functionally graded plates including thickness stretching effects, *Composite Structures*, Vol. 133, pp. 12, 2015.

[3] C. H. Thai, A. J. M. Ferreira, E. Carrera, H. N. Xuan, Isogeometric analysis of laminated composite and sandwich plates using a layerwise deformation theory, *Composite Structures*, Vol. 104, pp. 19, 2013.

[4] A. J. M. Ferreira, G. E. Fasshauer, R. C. Batra, J. D. Rodrigues, Static deformations and vibration analysis of composite and sandwich plates using a layerwise theory and RBF-PS discretizations with optimal shape parameter, *Composite Structures*, Vol. 86, pp. 16, 2008.

[5] C. M. C. Roque, J. D. Rodrigues, A. J. M. Ferreira, Static Deformations and Vibration Analysis of Composite and Sandwich Plates Using a Layerwise Theory and a Local Radial Basis Functions-Finite Differences Discretization, *Mechanics of Advanced Materials and Structures* Vol. 20, pp. 13, 2013.

[6] S. Farahmand, A. A. Atai, Parametric investigation of auto-frettage process in thick spherical vessel made of functionally graded materials, *Journal of Computational Applied Mechanics*, Vol. 47, No. 1, pp. 9, 2016.

[7] A. Afshin, M. Z. Nejat, K. Dastani, Transient thermoelastic analysis of FGM rotating thick cylindrical pressure vessels under arbitrary boundary and initial conditions, *Journal of Computational Applied Mechanics*, Vol. 48, No. 1, pp. 12, 2017.

[8] M. Goodarzi, M. N. Bahrami, V. Tavaf, Refined plate theory for free vibration analysis of FG nanoplates using the nonlocal continuum plate model, *Journal of Computational Applied Mechanics*, Vol. 48, No. 1, pp. 14, 2017.

[9] M. Gharibi, M. Z. Nejad, A. Hadi, Elastic analysis of functionally graded rotating thich cylindrical pressure vessels with exponentially varying properties using power series method of frobenius, *Journal of Computational Applied Mechanics*, Vol. 48, No. 1, pp. 10, 2017.

[10] J. L. Mantari, A. S. Oktem, C. G. Soares, Static and dynamic analysis of laminated composite and sandwich plates and shells by using a new higher-order shear deformation theory, *Composite Structures*, Vol. 94, pp. 13, 2011.

[11] H. N. Xuan, C. H. Thai, T. N. Thoi, Isogeometric finite element analysis of composite sandwich plates using a higher-order shear deformation theory, *Composites: Part B*, Vol. 55, pp. 17, 2013.

[12] M. Goodarzi, M. Mohammadi, M. Khooran, F. Saadi, Thermo-mechanical vibration analysis of FG circular and annular nanoplate based on the visco-pasternak foundation, *journal of Solid Mechanics*, Vol. 8, No. 4, pp. 18, 2016.

[13] M. R. Farajpour, A. Rastgoo, A. Farajpour, M. Mohammadi, Vibration of piezoelectric nanofilm based electromechanical sensors via higher order nonlocal strain gradient theory, *IET Micro & Nano Letters*, Vol. 11, No. 6, pp. 6, 2016.

[14] A. Farajpour, A. Rastgoo, M. Mohammadi, Surface effects on the mechanical characteristics of microtubule networks in living cells, *Mechanics Research Communications*, Vol. 57, pp. 9, 2014.

[15] A. Farajpour, M. Danesh, M. Mohammadi, Buckling analysis of variable thickness nanoplates using nonlocal continuum mechanics, *Physica E*, Vol. 44, pp. 9, 2011.

[16] A. Farajpour, M. R. H. Yazdi, A. Rastgoo, M. Loghmani, M. Mohammadi, Nonlocal Nonlinear plate model for large amplitude vibration of magneto-electro-elastic nanoplates, *Composite Structures*, Vol. 140, pp. 14, 2015.

[17] M. Mohammadi, A. Farajpour, A. Moradi, M. Ghayour, Shear buckling of orthotropic rectangular graphene sheet embedded in an elastic medium in thermal environment, *Composite: Part B*, Vol. 56, pp. 9, 2014.

[18] M. Mohammadi, A. Farajpour, M. Goodarzi, H. S. n. pour, Numerical study of the effect of shear in plane load on the vibration analysis of graphene sheet embedded in an elastic medium, *Computational Materials Science*, Vol. 82, pp. 11, 2014.

[19] M. Mohammadi, M. Ghayour, A. Farajpour, Free transverse vibration analysis of circular and annular graphene sheets with various boundary conditions using the nonlocal continuum plate model, *Composite: Part B*, Vol. 45, pp. 11, 2013.

[20] A. Farajpour, M. R. Haeri, A. Rastgoo, M. Mohammadi, A higher order nonlocal strain gradient plate model for buckling of orthotropic nanoplates in thermal environment, *Acta Mech*, Vol. 227, pp. 19, 2016.

[21] P. Ghabezi, M. Farahani, Composite adhesive bonded joint reinforcement by incorporation of nano-alumina particles, *Journal of Computational Applied Mechanics*, Vol. 47, No. 2, pp. 9, 2017.

[22] S. J. Lee, H. R. Kim, FE analysis of laminated composite plates using a higher-order shear deformation theory with assumed strains, *Latin American Journal of Solids and Structures*, Vol. 10, pp. 25, 2013.

[23] M. S. A. Houari, A. Tounsi, A. Beg, Thermoelastic bending analysis of functionally graded sandwich plates using a new higher-order shear and normal deformation theory, *International Journal of Mechanical Sciences* Vol. 76, pp. 10, 2013.

[24] M. Meunier, R. A. Shenoi, Dynamic analysis of composite sandwich plates with damping modelled using high-order shear deformation theory, *Composite Structures*, Vol. 24, pp. 12, 2001.

[25] M. Shishesaz, M. Kharazi, P. Hosseini, M. Hosseini, Buckling behavior of composite plates with a pre-central circular delamination defect under in plane unaxial compression, *Journal of Computational Applied Mechanics*, Vol. 48, No. 1, pp. 12, 2017.

[26] C. H. Thai, A. J. M. Ferreira, M. A. Wahab, H. N. Xuan, A generalized layerwise higher-order shear deformation theory for laminated composite and sandwich plates based on isogeometric analysis, *Acta Mech*, Vol. 227, pp. 26, 2016.

[27] S. Sarangan, B. H. Singh, Higher-order closed-form solution for the analysis of laminated composite and sandwich plates based on new shear deformation theories, *Composite Structures*, Vol. 138, pp. 13, 2016.

[28] S. Srinivas, A. K. Rao, Bending, Vibration and Buckling of simply supported thick orthotropic rectangular plates and laminates, *International Journal of solid structures*, Vol. 6, pp. 19, 1970.

[29] H. H. Abdelaziz, H. A. Atmane, I. Mechab, L. Boumia, A. Tounsi, A. B. E. Abbas, Static Analysis of Functionally Graded Sandwich Plates Using an Efficient and Simple Refined Theory, *Chinese Journal of Aeronautics*, Vol. 24, pp. 15, 2011.

[30] H. Cease, P. F. Derwent, H. T. Diehl, J. Fast, D. Finley, Measurement of mechanical properties of three epoxy adhesives at cryogenic temperatures for CCD construction, *Fermilab-TM*, 2006.

[31] L. D. Peel, Exploration of high and negative Poisson's ratio elastomer-matrix laminates, *Physica status solidi (b)*, Vol. 244, pp. 16, 2007.

[32] V. Gonca, Definition of poissin's ratio of elastomers, Engineering for rural development, in *10th International scientific conference Engineering for Rural Development*, Jelgava, Latvia, 2011.